Key Points:
- The number of accidents due to warmer snow cover has increased
- The forces that can damage engineered structures can be approximated
- Water under pressure underneath snowpacks is key to triggering glide avalanches

Supporting Information:
- Text S1
- Figure S1
- Figure S2
- Figure S3
- Figure S4
- Figure S5
- Figure S6a
- Figure S6b
- Figure S7
- Figure S8
- Figure S9
- Figure S10
- Figure S11
- Figure S12
- Figure S13
- Figure S14
- Figure S15

Correspondence to:
C. Ancey,
christophe.ancey@epfl.ch

Dynamics of glide avalanches and snow gliding

Christophe Ancey[1] and Vincent Bain[2]

[1] Laboratory of Environmental Hydraulics, School of Architecture, Civil and Environmental Engineering, École Polytechnique Fédérale de Lausanne, Lausanne, Switzerland, [2] Toraval, Les Favrets, Héry-sur-Ugine, France

Abstract In recent years, due to warmer snow cover, there has been a significant increase in the number of cases of damage caused by gliding snowpacks and glide avalanches. On most occasions, these have been full-depth, wet-snow avalanches, and this led some people to express their surprise: how could low-speed masses of wet snow exert sufficiently high levels of pressure to severely damage engineered structures designed to carry heavy loads? This paper reviews the current state of knowledge about the formation of glide avalanches and the forces exerted on simple structures by a gliding mass of snow. One particular difficulty in reviewing the existing literature on gliding snow and on force calculations is that much of the theoretical and phenomenological analyses were presented in technical reports that date back to the earliest developments of avalanche science in the 1930s. Returning to these primary sources and attempting to put them into a contemporary perspective are vital. A detailed, modern analysis of them shows that the order of magnitude of the forces exerted by gliding snow can indeed be estimated correctly. The precise physical mechanisms remain elusive, however. We comment on the existing approaches in light of the most recent findings about related topics, including the physics of granular and plastic flows, and from field surveys of snow and avalanches (as well as glaciers and debris flows). Methods of calculating the forces exerted by glide avalanches are compared quantitatively on the basis of two case studies. This paper shows that if snow depth and density are known, then certain approaches can indeed predict the forces exerted on simple obstacles in the event of glide avalanches or gliding snow cover.

1. Introduction

Climate change has a significant impact on the frequency and intensity of gravity-driven flows (e.g., snow avalanches and debris flows) due to its effects on snow melt, glacier retreat, runoff regimes, frozen soil (permafrost), sediment production, timber line altitude, etc. [*Beniston*, 2003; *Adam et al.*, 2009; *Bebi et al.*, 2009; *Keiler et al.*, 2010; *Stoffel and Huggel*, 2012]. Climate change is therefore likely to influence the occurrence of damage due to avalanches; however, the exact trend remains undecided and will be highly dependent on the region concerned [*Lavigne et al.*, 2012; *Castebrunet et al.*, 2012; *McClung*, 2013]. Some studies have concluded that there is no clear correlation between the frequency of extreme events and climatic conditions [*Schneebeli et al.*, 1998; *Eckert et al.*, 2010a], whereas others have provided evidence that the runout distance of extreme avalanches has decreased since the mid-1970s [*Eckert et al.*, 2010b]. A few studies have reported increased avalanche activity in recent years [*Valt and Paola*, 2013]. Regional climate models predict an increase in wet-avalanche activity in the 21st century [*Castebrunet et al.*, 2014].

Climate change poses numerous challenges to risk management. One emerging issue is the perceived increase in the frequency of accidents due to wet-snow avalanches, especially *glide avalanches* (a particular form of wet-snow avalanches, defined below). To the best of our knowledge, although field surveys to date have shown the considerable variability in the nature of avalanche activity in recent decades (at least until the 2000s), they have not revealed any clear trend between global warming and the frequency of wet-snow avalanches [*Baggi and Schweizer*, 2009]. However, in recent years, numerous accidents caused by gliding snowpacks and glide avalanches have been observed. For instance, although the 2011–2012 and 2012–2013 winters experienced very different snowpack formation conditions, both were associated with glide avalanche activity [*Mitterer and Schweizer*, 2012; *Pielmeier et al.*, 2013]. As some of these recent events happened in areas not usually exposed to avalanches, the question arose as to whether avalanche risk maps should be updated to take this "new" threat into account [*Margreth*, 2013]. The incredibly high pressures exerted by snow and documented at some damaged facilities are further grounds for concern. For instance, during the snowy winter of 1998–1999, the foundations of a chairlift tower in Elm (Switzerland) slipped 8 m
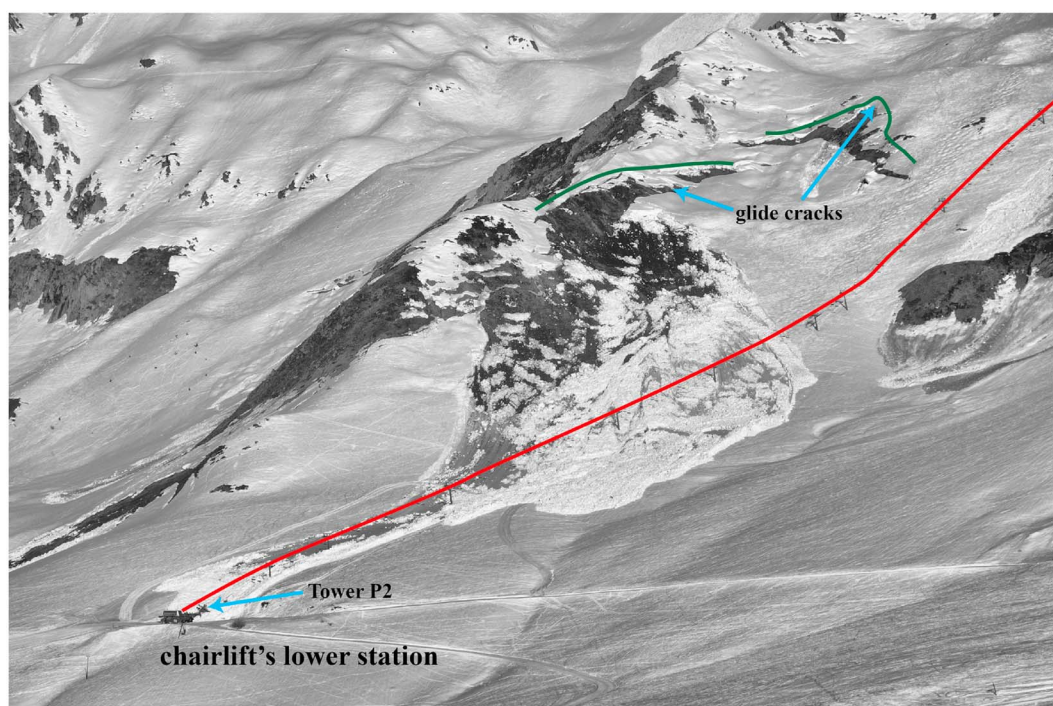
Figure 1. View of the avalanche path and the chairlift hit by the 2 March 2012 avalanche at Saint-François-Longchamp. Tower P2, near the lower station, was bent at its base. Two wide glide cracks can be seen on the upper part of the slope (others are also visible in many places). The crack farthest to the right did not generate an avalanche, whereas the crack farthest to the left led to the glide avalanche that damaged the chairlift.

downhill under the effects of gliding snow. A back calculation of the forces exerted by the snowpack on the tower led to snow pressure estimates as high as 500 kPa [*Ammann*, 2000].

There is a tremendous body of work on the calculation of snow forces, including those generated by wet snow. Historically, in avalanche-prone regions, inhabitants showed great awareness about the threat of avalanches and coped with this by building their dwellings in relatively secure areas, often behind the protection of dense forests and sometimes earth barriers [*Laternser and Pfister*, 1997; *Rabusseau*, 2007; *Ancey*, 2015]. In the nineteenth century, engineers tried different techniques, including forestation and erecting man-made obstacles composed of stakes and stone walls in starting zones in order to halt avalanche release. As André Roch summarized, many of these attempts caused bitter disappointment [*Roch*, 1980]. In 1860, for instance, in Barèges, French military engineers covered starting zones with bench terraces and planted an artificial forest of stakes and wooden fences [*Campagne*, 1905], yet within 10 years strong winds and heavy snow loads had knocked this forest down. In Switzerland and Austria, kilometers of terraces and stone walls were built between the late nineteenth and early twentieth centuries [*Fankhauser*, 1920; *Sauermoser et al.*, 2011], and the earliest snow rakes were tested too [*Mougin*, 1913; *Sulzlée*, 1950]. However, many of these works suffered from poor design and were rapidly damaged by snow loads and avalanches. It was not until 1936, with the creation of the Federal Institute for Snow and Avalanche Research (SLF) in Davos, that snow mechanics and avalanche formation started to be studied using both laboratory experiments and field surveys, thus giving a more consistent scientific framework for designing defensive structures. The original avalanche protection guidelines written by Robert Haefeli and his colleagues have been gradually updated. Today, they are referred to as the *Swiss guidelines* and are used worldwide [*Margreth*, 2007a].

This paper aims to review the state of the art of snow pressure calculations for gliding snowpacks and glide avalanches. There is a considerable existing body of work on these topics, and although the precise physical mechanisms governing gliding snow are still only partially understood, current computational methods do, in fact, provide fairly good estimates of the forces involved. In the two case studies presented in this paper, we decided to focus on simple structures (cylindrical obstacles such as chairlift towers), essentially not only
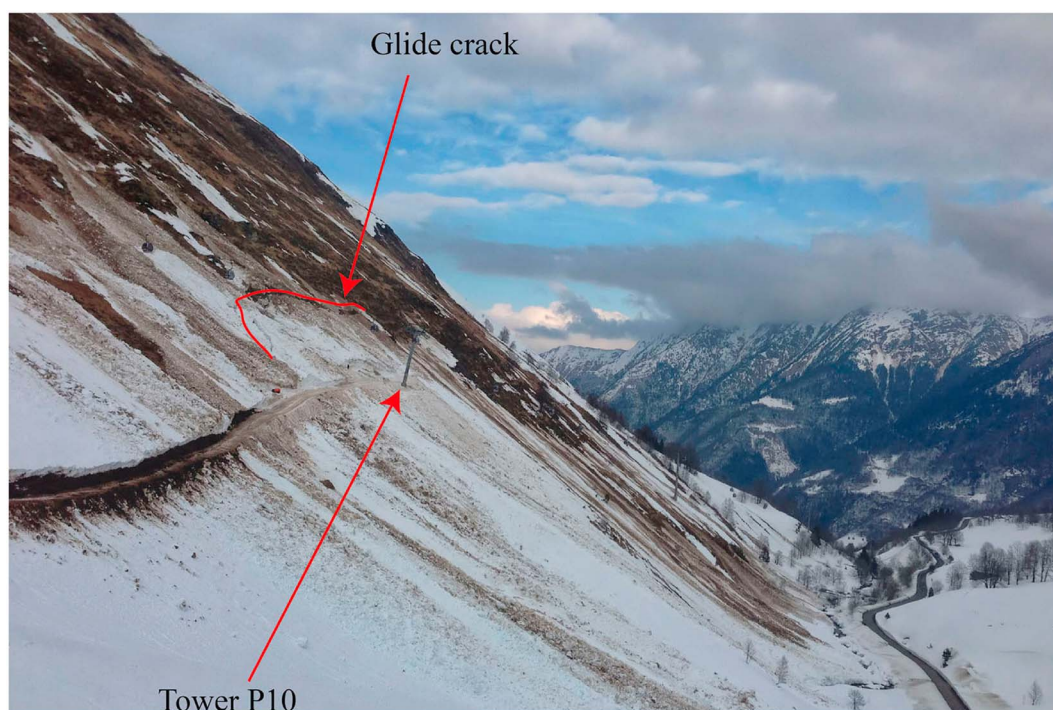
Figure 2. Side view of tower P10 on 18 February 2013. The glide crack is about 60 m uphill from the tower. A track was dug for the rescue operation. Courtesy of J.-L. Pons.

because of the availability of data and observations but also for the relatively greater ease in back calculating snow pressure.

In the supporting information, we present two case studies of damage which occurred to ski lifts in France.

1. On 2 March 2012, a glide avalanche induced by a mild spell of weather damaged a chairlift tower in Saint-François-Longchamp, a ski resort in the French Alps (see the tourist-made video on https://www.youtube.com/watch?v=8eXKi6aiGlg). Figure 1 shows the avalanche path and its deposit near the chairlift's lower station (1900 m). The glide avalanche originated from an apparently consolidated glide crack which had started to develop in early January. The slope angle just below the ridge line was quite steep (4° between 2100 m and 2050 m) but quickly became gentler (30° between 2050 m and 1950 m). A thick slab started to slip on the grassy slope; its initial surface was approximately 1.1 ha, and its mean thickness was about 2.5 m, leading to an initial snow volume of about 25,000 m^3.

2. On 16 February 2013, a cable car tower was tipped over by a gliding snow slab in Cauterets, a ski resort close to the Franco-Spanish border. Figure 2 shows the compact snow slab resulting from the deposits of numerous avalanches caused by heavy snowfall (10 m within 1 month at 1850 m); its slow slip (maximum 4 m d^{-1}) exerted so much pressure on the tower that it was bent at its base.

Part 1 of this review begins with a phenomenological description of gliding snow and glide avalanches in order to define the terms used below, describe the physical features of each phenomenon, and give indications on the level of damage incurred in France and Switzerland (see section 2). We will examine the snow conditions that lead to the formation of a glide avalanche (see section 3). This problem is of paramount importance to ski resorts (for predicting occurrences of glide avalanches) and avalanche prevention professionals (for mitigating the risk of glide avalanches by intervening directly in their starting zones).

Part 2 is devoted to the calculation of the forces exerted by gliding snow, or a glide avalanche, on a narrow obstacle such as a lift tower. We first review calculations of the forces generated by a gliding/creeping snowpack (see section 4). This is a classic problem, but it has given rise to lively debates. Indeed, as the mechanical behavior of snow is notoriously difficult to model, the only way to make progress on this issue has long been seen to be great simplification of reality—retaining only the salient features of the real system. For instance, the assumptions adopted for estimating snow forces in the Swiss guidelines [*Margreth*, 2007a] have been

seen as oversimplified [*McClung*, 1993]. For this reason, we have attempted to outline each approach not only by discussing their physical assumptions (together with their strengths and weaknesses) but also by adapting their governing equations into forms that are consistent with current standards in mechanics. In section 5, we review the different approaches to calculating the force exerted by a glide avalanche on a narrow obstacle. As glide avalanches are a particular form of wet avalanche, much of the knowledge is drawn from studies on wet-avalanche dynamics. This problem has been the subject of renewed interest in recent years. Certain researchers stated that if such unexpectedly high pressures were recorded for wet-snow avalanches, then doubts should be cast on the computational methods used in engineering. Such claims were perhaps excessive—they came close to denying the results of a large body of empirical work—and inevitably pro-voked a backlash, but a more gradual transformation in views is now taking place thanks to high-resolution field measurements and a deeper understanding of the dynamics of granular and plastic flows. Section 6 compares the different approaches when applied to the two case studies.

An explanatory list of the notation used in this paper accompanies the appendices. The two case studies are presented at length in the supporting information. The supporting information also includes additional information about the effects of global warming on snowpacks and avalanche activity.

2. Snow Gliding and Glide Avalanches

2.1. Definitions

Snow gliding and glide avalanches remain the major stumbling blocks in our understanding of avalanches and related processes. On the one hand, observations are abundant: they have already been described at length in the earlier avalanche studies [*Coaz*, 1881; *Mougin*, 1922; *Allix*, 1925], and the terminology was estab-lished a long time ago [*de Quervain*, 1965, 1981]. On the other hand, the picture of what precisely is happening at a physical level is still blurred. In particular, a clear and consensual synthesis of the underlying mechanisms of slip is still lacking. Here we provide a phenomenological description of snow gliding and glide avalanches which serves as the basis for the analyses below. We do not enter into the details of the physical processes as these are discussed in section 3. We also refer readers to the review papers by *Jones* [2004] and *Höller* [2012], who have summarized a century of worldwide observations and the corresponding efforts at modeling.

When snow lies on a sloping surface, gravitational forces cause the snow to creep: the snowpack undergoes vertical strains (snow compaction due to metamorphism and settlement) and shear strain (displacement par-allel to the slope). *Creeping* is a process common to all materials exhibiting viscous-like behavior, and—even for compressible materials like snow—it is therefore not considered to contribute insurmountable problems in terms of modeling. Another mode of snowpack displacement is called *gliding*. Under certain conditions, the entire snowpack may slip downhill at a slow velocity; i.e., the usual no-slip condition for flows over impermeable rigid surfaces is violated.

2.2. Snow Gliding

Even though the bigger picture remains elusive, field observations from the 1920s onward have shown that gliding is mostly observed under very specific conditions [*in der Gand and Zupančič*, 1965; *Frutiger and Kuster*, 1967; *McClung*, 1975; *Mellor*, 1978; *Endo*, 1984; *Lackinger*, 1986; *McClung and Clarke*, 1987; *McClung et al.*, 1994; *Clarke and McClung*, 1999; *Newesely et al.*, 2000; *Leitinger et al.*, 2008; *Höller et al.*, 2009; *Stimberis and Rubin*, 2011; *Peitzsch et al.*, 2012; *Mitterer and Schweizer*, 2012; *Dreier et al.*, 2013; *Viglietti et al.*, 2013; *Peitzsch et al.*, 2014; *Feistl et al.*, 2014; *Meusburger et al.*, 2014]: (i) slope angle must be sufficiently steep, typically greater than 28°, but slopes as low as 15° have also been cited; (ii) ground must be sufficiently smooth and free of obsta-cles, typically an open grassy slope or bare rock, but snow gliding is also observed under sparse forest cover; (iii) free water must be present at the ground/snow interface, which implies that the ground temperature must be 0°C or higher; however, some studies have also pointed out that an isothermal snowpack (at 0°C across its entire depth) is a prerequisite, which greatly influences both the type of snow crystals (rounded grains) and the stress distribution within the cover. Studies show the absence of correlation between daytime and night-time rates of snow glide as well as the possible occurrence of significant gliding rates with cold temperatures [*Clarke and McClung*, 1999].

Glide rates can be highly variable from one season to another, even at the same location. For instance, a field survey conducted over 11 winter seasons above Amden (Switzerland), at 1540 m, showed that the snow cover on a 40° slope traveled between 19 and 102 cm per season [*Ammann*, 2000; *Margreth*, 2007b]; the average glide rate was about 50 cm per season, i.e., a few millimeters per day. On some occasions,

a complex combination of meteorological and snowpack conditions may lead to increased glide rates. When this happens, rates of a few centimeters per day have frequently been observed [*Clarke and McClung*, 1999], but extreme values as much as 43 to 67 cm/h have also been reported [*Margreth*, 2007b; *Stimberis and Rubin*, 2011; *Caduff et al.*, 2015].

Snow gliding probably reflects the local interplay between the snowpack and ground, and so rates at specific locations may vary significantly depending on topography. The differences in glide rates between areas of snow cover close to one another may generate large tensile stresses within the snowpack, and once a critical level of stress is reached, the snow cover develops a *glide crack*, i.e., a tensile fracture across the entire snow depth. This explains why glide cracks are mostly observed at the same locations from one season to another. Figure 1 shows glide cracks in Saint-François-Longchamp.

As pointed out by *Clarke and McClung* [1999], the rupture and release of the snowpack are more likely to be consequences of increased glide rates than of a threshold glide rate (the latter process has been suggested by *in der Gand and Zupančič* [1965]). The ground and crown surfaces are approximately perpendicular, which is interpreted as the result of reduced bottom shear and increased tensile stresses in the cracking region [*McClung*, 1986]. Viewed from above, glide cracks often form arc-shaped crevasses (called *avalanche mouths*), which may extend over a few tens of meters.

2.3. Water Through Snow

Snow is an unsaturated porous medium [*Denoth*, 1982; *Colbeck*, 1986; *Brun*, 1989; *Marsh*, 1991, 2005]. Dry snow is a two-phase material (air and ice), whereas for wet snow, there is also liquid water occupying part of the interstitial space. The amount of water available in the liquid state is usually expressed as the *liquid water content* $W = V_w/V$, which is the volume occupied by liquid water V_w relative to the total volume V, and the *liquid saturation* $S_w = W/\phi_s$, where ϕ_s denotes snow porosity (the fraction of void space in the snow volume). In porous media composed of a granular skeleton, such as snow, how liquid water is distributed within the pores depends primarily not only on the liquid saturation but also on the shape of the grains [*Szymkiewicz*, 2013].

When liquid saturation is very low (usually $S_w < 3\%$ for old snow), liquid water concentrates in the acute corners of the pores. It forms rings (capillary bridges) around the contact points between grains. It may also form films covering the grains' surfaces. The solid-ice skeleton is thus characterized by clusters of ice grains held together by capillary forces (the liquid bonds undergo melt-freeze cycles under certain conditions of heat flux). Surface tension is sufficiently large for this liquid water to be held in place. Air flow occurs in a continuous path through the snow. When more water is added (as a result of either rainfall or snow melt), the water films surrounding the grains coalesce, forming a continuous, thicker film that slowly drains away under the effect of gravity. This situation, characterized by low to moderate liquid saturation ($S_w < 11 – 14\%$), is called the *pendular regime* and corresponds to freely draining snowpacks; the water that is free to flow through the pores is called *free water*. In terms of liquid water content, this occurs when W is in the 3% – 7% range.

When the liquid saturation is high (usually when $S_w > 14\%$ for old snow), the ice grains are completely surrounded by water, whereas the air is trapped in bubbles within the pores. Saturation of the pore space occurs where there is a low-permeability boundary, such as the ground or an ice crust buried in the snow. This stage is called the *funicular regime*. As snow covers are heterogeneous (as a result of stratification, spatial variability in snow permeability, etc.), the funicular regime leads to free water following preferential flow paths [*Colbeck*, 1974a; *Marsh*, 2005; *Techel and Pielmeier*, 2011; *Walter et al.*, 2013].

2.4. Glide Avalanche Initiation

A glide crack can cause a glide avalanche to occur. Initially, a glide avalanche is a full-depth avalanche, i.e., a snow slab that slips along the ground (see Figure 1). For a glide avalanche to occur, the base of the snowpack must be wet. Its snow contains sufficiently high liquid water content (up to 3 – 7%) for free water to be able to percolate down to the lowermost layers of the snow cover [*McClung and Schaerer*, 1993]. The upper part of the snow cover is mostly wet but sometimes can be composed of dry snow (e.g., new snow).

Once a glide crack has developed and formed the crown of the slab, the strength of its lower bound (called the *stauchwall*) can play an important part in the probability of release [*Lackinger*, 1986; *Bartelt et al.*, 2012]. The lag time between crack initiation and slab release ranges from a few hours to a few weeks. It seems to be highly correlated with air temperature and the degree of snowpack settlement [*Reardon et al.*, 2006; *Peitzsch et al.*, 2012; *Dreier et al.*, 2013]. In his field survey above Innsbruck, *Lackinger* [1986, 1988] pointed out that
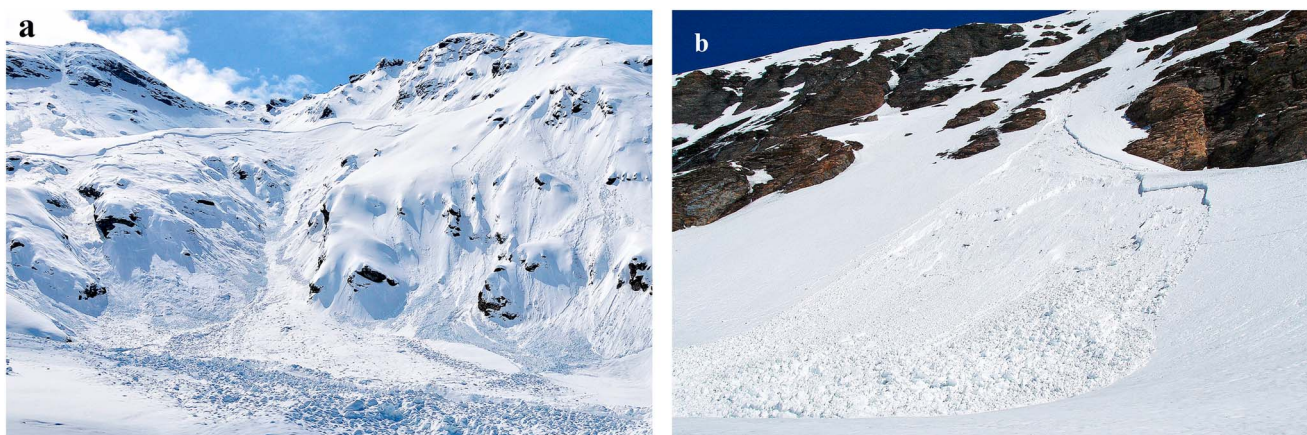
Figure 3. Fracture lines. (a) Wet-slab avalanche (Valcenis, France, April 2009). The fracture thickness was about 1 m on average. The avalanche brought down 200,000 m^3 of snow. (b) Loose-snow avalanche (Grand Roc Noir, France, March 2005) initiating at one point. Note the typical triangular shape of the flanks. This avalanche brought down less than 100 m^3 of snow.

many glide avalanches occurred in the late afternoon and overnight, which implies that refreezing may lead to stress redistribution within the snowpack and a change in the circulation of free water. *Clarke and McClung* [1999] also observed the occurrence of glide avalanches with cold temperature.

2.5. Glide Avalanche Motion

After release, glide avalanches behave like wet-snow avalanches. Wet-snow avalanches form a class of avalanches, all of which result from the release of either a wet slab (i.e., the snowpack is wet across its entire depth) or a loose wet-snow volume, which initiates at one specific point and grows larger as it goes downhill [*McClung and Schaerer*, 1993]. Figure 3a shows a typical wet-slab avalanche, whereas Figure 3b presents a loose wet-snow avalanche. In both cases, the liquid water content is sufficiently high (>3%) and snow temperature is 0°C [*Techel and Pielmeier*, 2011; *Mitterer*, 2012]. This small amount of liquid water is sufficient to cause significant changes in the snow's composition (e.g., formation of snowballs) and rheological behavior (usually characterized by higher-energy dissipation rates) [*Steinkogler et al.*, 2014]. Figure 4 shows two typical examples of wet-snow avalanche deposits: during its course, the avalanche causes snow to compact and form rounded snowballs, the size distribution of which depends on the liquid water content, snow temperature, and duration of the flow (see Figure 4a). When the liquid water content is very high (> 8%), snow deposits are often very compact, with densities as high as 550 kg m^{-3} (see Figure 4b). The velocity reached by wet-snow avalanches on mild slopes is usually low, with a typical magnitude of about 1 m s^{-1} (by comparison, extreme snow gliding rates are close to 2 mm s^{-1} while dry-snow avalanches reach much higher velocities, usually higher than 10 m s^{-1}).

Glide avalanches are mostly composed of wet snowpacks, but on occasion the upper part of the snow cover can be composed of dry snow. In such cases, when the snow cover breaks, the layers start to slide downhill in the form of a cohesive slab, but this quickly smashes into thousands of chunks which form wet snow as
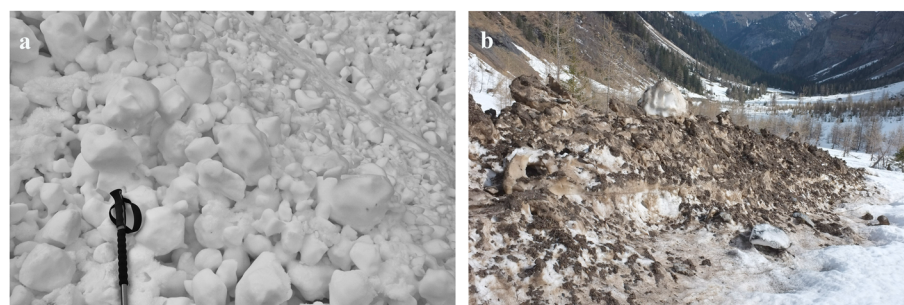

Figure 4. Snow deposits from wet avalanches. (a) Rounded snow balls (Col du Jorat, Switzerland, February 2011); the typical diameter of snow granules was 20 cm. (b) Compact wet-snow deposit covered with debris (Col Champion, Switzerland, May 2013); the deposit thickness was 1.5 m on average.
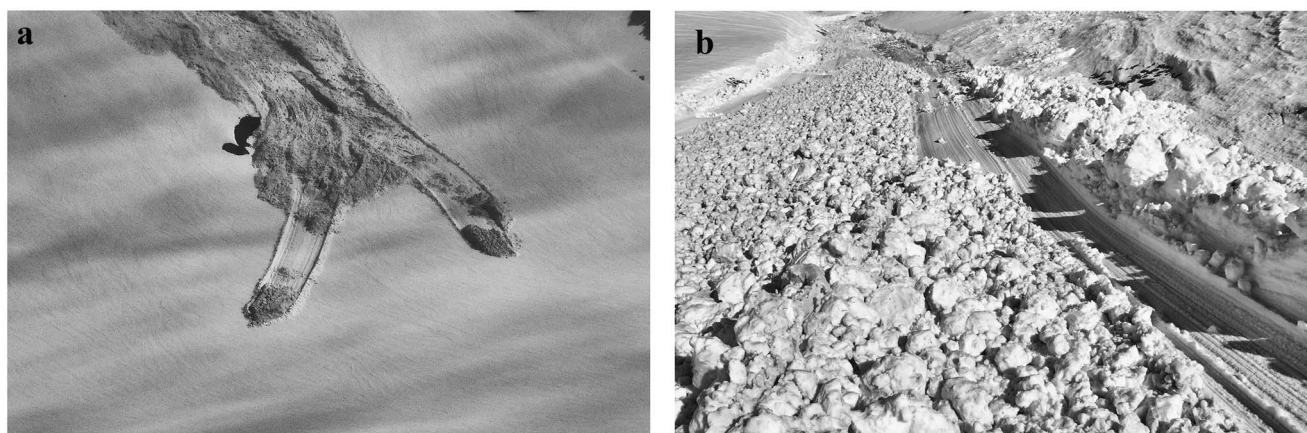
Figure 5. Paths of wet-snow avalanches. (a) The avalanche was confined between lateral levees created by the front (Cheval Blanc, Switzerland, May 2013); the levee height was about 1 m. (b) The avalanche gouged down into the snowpack and also formed lateral levees (Grammont, Switzerland, December 2008); the scouring depth was 30–50 cm.

they mix. For this reason, even if the mechanisms of release differ between glide avalanches and genuine wet avalanches, their flow behavior is the same owing to the internal mixing which they undergo.

Glide avalanches may drag along the entire snow cover—sometimes causing soil erosion as they drag along the superficial soil layer [*Meusburger et al.*, 2014]—or slip on top of another snow layer. Like other forms of wet-snow avalanche, they usually experience higher flow resistances than dry-snow avalanches. This explains why, on most occasions, they run shorter distances and reach lower velocities than high-speed dry-snow avalanches. However, on occasion, they can travel as far as high-speed avalanches and flow down shallow slopes. This scenario can be observed when their lateral spread is limited by terrain features or as the result of levee formation. Indeed, in the former case, glide avalanches can dig out a channel through the snow cover or follow an incision in the terrain (e.g., a gully, river bed, or a depression caused by torrential erosion) (see Figure 5a). In the latter case, they can form lateral deposits (levees) that confine any ensuing flow. These levees are formed by grain sorting (a process called *particle size segregation*): wet snow forms rounded snow-balls of different sizes; the largest snowballs concentrate in the fast-moving upper layers (next to the free surface of the avalanche) and are transported to the leading edge; from here they are pushed to the sides by the core of the avalanche (made up of the finest snowballs), which creates static coarse-grained levees (see Figure 5b). This self-organization has a great influence on the flow's behavior as it reduces the dissipative effects of frictional forces.

The traditional view is that most catastrophic avalanches follow the same basic principle: fresh snow accumulates on a mountain slope until the gravitational force at the top of the slope exceeds the binding force holding the snow together, resulting in the release of a snow slab. Catastrophic avalanches are thus mostly associated with dry snow, heavy snowfall, and high speeds. There is, however, clear evidence from the field that for certain sites, wet-snow avalanches are the major threat. Typical examples include the Saint-Clément avalanches at Tours-en-Savoie (France), where avalanches traveled long distances down shallow slopes (<10%) and deposited large accumulations of wet snow (exceeding 10^6 m^3) on the valley floor [*Gex*, 1923; *Ancey*, 2012a]. If a generalized Coulomb friction model, such as the Voellmy model, is used to compute that avalanche's runout distance, the friction parameter μ would have to have been as low as 0.08; however, *Salm et al.* [1990] give 0.155 as the minimum friction value for extreme avalanches. This behavior can be observed for both high- and low-volume avalanches [*Ancey and Meunier*, 2004; *Ancey*, 2005].

2.6. Damage and Economic Costs

In terms of damage to dwellings and infrastructure (ski lifts and power lines), gliding snow and glide avalanches are usually a minor threat relative to those caused by dry-snow and other forms of wet-snow avalanches. *Lackinger* [1986] cited the Schmalzberg (Vorarlberg, Austria) avalanche of 31 December 1974, with a death toll of 12 villagers. A survey of Swiss ski areas (with a total of 1800 ski lifts) between 1996 and 2007 documented three cases of damage to ski lifts [*Margreth*, 2007b], but in the winter of 2011–2012 alone, there were 88 accidents due to glide avalanches in Switzerland [*Techel et al.*, 2013]. That same winter, a tower supporting a chairlift at Lungern-Schönbüel was tipped over by gliding snow in late January, while a glide
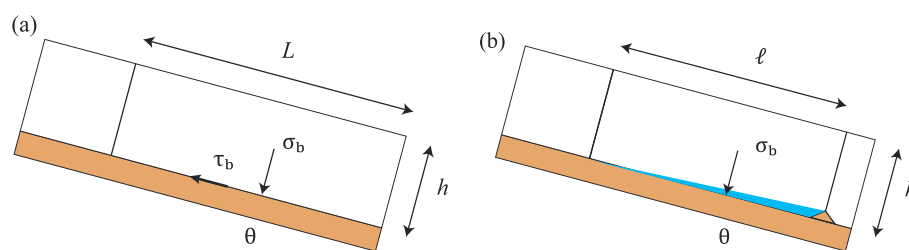
Figure 6. (a) Slab geometry considered by Haefeli and subsequent authors: a slab of uniform depth h and length L is resting on sloping ground. (b) In Lackinger's model, there are patches of length ℓ, whose basal resistance is significantly reduced by water under pressure.

avalanche damaged a ski lift in Ovronnaz in late February. In France, with a total of 3400 ski lifts, the survey we conducted in spring 2013, questioning the main infrastructure managers, reported six accidents due to snow gliding in the last 20 years: Avoriaz (spring 1995), Foux d'Allox (February 1997), Morillon (May 2000), Contamines (spring 2012), Cauterets (February 2013), and Luz-Ardiden (February 2013). Two other accidents due to glide avalanches are also known: in the evening of 21 March 1971, a glide avalanche damaged five buildings at La Grave (Chazelet) without causing any injuries (occupants had time to evacuate their houses as snow penetrated windows and doors) [*Ancey*, 1996], and the 2 March 2012, avalanche in Saint-François-Longchamp, as described in this paper (the same chairlift experienced another accident on 9 March 2014).

In mountainous regions, repeated damage to forests, defense structures in starting zones, roads, equipment, and buildings represent nonnegligible financial costs to landowners, ski resorts, municipalities, and companies. However, they remain difficult to quantify in money terms except in certain Swiss cantons where one can draw on centralized data from public building insurance companies. The costs incurred by insurance companies due to the damage sustained in those cantons in the winter of 2011–2012 were estimated at 20 million Swiss Francs (for the disastrous winter of 1998–2099 costs amounted to about 100 million).

3. Glide Avalanche Initiation

Decades of observations have formed the dominant view that glide avalanches result from a significant drop in basal friction induced by free water within isothermal snowpacks [*Höller*, 2012]. However, there is a lack of understanding on the exact mechanism whereby water "lubricates" the interface between the sliding snowpack and ground. To date, the analysis of the release of glide avalanches has mostly concerned the simplest case (see Figure 6a): a snow cover of uniform depth h extends to infinity, both laterally and in the downward direction, over a terrain inclined at an angle θ. If there is a significant decrease in the bottom shear stress τ_b over a sufficiently long distance L, then the reduction of basal friction is counterbalanced by an increase in tensile stresses, which may lead to the initiation of the glide crack. Release and subsequent motion of the slab still require low basal friction. So the crux of the problem is the proper determination of what happens at the interface between the snowpack and ground.

3.1. Mechanisms of Incipient Motion: Physical Considerations

Let us consider a uniform layer of a material (be it solid or fluid) initially at rest on a sloping bed. For a stationary, uniform layer, the stress distribution is given as $\tau_b = \rho g h \sin\theta$ and $\sigma_b = -\rho g h \cos\theta$, where ρ denotes the bulk density, g is the gravitational acceleration, h is the layer's thickness, and θ is the bed inclination (see Figure 6a). Under certain circumstances, this layer starts slipping or flowing downward as a result of gravitational forces. This is a classic geomechanical and geomorphological problem in the study of slope stability and intermittent motion; it helps us to understand the basic mechanisms of flow initiation and propagation for landslides, debris flows, submarine avalanches, glaciers, and avalanches. Various approaches have been developed depending on (i) whether the material is seen as homogeneous or heterogeneous (e.g., a saturated granular material) and (ii) whether the bulk material behaves as a fluid or as a solid.

Usually, most homogeneous fluids satisfy the no-slip condition at the bottom, but even in the comfortable environment of the laboratory, the specific interactions between a material and a solid boundary remain poorly understood and a matter of fierce debate; this is especially true for non-Newtonian fluids [*Barnes*, 1995]. For many fluids, high-resolution experiments have shown that the no-slip condition can be violated at the microscopic level, although it successfully expresses flow behavior near the boundary at the macroscopic

scale [*Neto et al.*, 2005]. Several mechanisms (e.g., strong physicochemical fluid-solid interactions, nanobubbles, or shark skin effects) have been proposed in attempts to elucidate the appearance of wall slip in simple fluids [*Sochi*, 2011], but they concerned industrial fluids rather than natural materials. Slip may occur also within yield stress fluids: when the shear stress exceeds a critical value called the yield stress τ_c, the material starts flowing along the yield surface $y = h - \tau_c/(\rho g \sin \theta)$ [*Barnes*, 1999]. Yield stress fluids have long been used to model natural materials such as debris mixtures and snow [*Johnson*, 1970; *Ancey*, 2007]. However, this ideal situation poses theoretical problems for the slope stability problem addressed here [*Thual and Lacaze*, 2010], and its suitability as a rheological model for debris flows has been questioned [*Iverson*, 1997]. This model's major deficiency is the absence of general mechanism to explain how a stable layer of material becomes unstable or, to put it differently, why the yield stress decays sufficiently for the layer to yield. One possible mechanism to explain slope failure is the dissolution of the clay bonds linking coarse particles [*Bardou et al.*, 2007]; however, this is very specific to materials with a sufficient clay content.

The current trend in geophysical fluid dynamics is to regard natural materials as two-phase materials, i.e., heterogeneous granular mixtures, whether or not they are fully saturated by an interstitial fluid [*Iverson and Vallance*, 2001]. The simplest model (borrowed from geomechanics) is that of a saturated frictional Coulomb. The bottom shear stress is then expressed as a function of the bottom normal stress σ_b and pore pressure p (see Figure 6a): $\tau_b = \mu(\sigma_b - p)$ where μ denotes the Coulomb friction coefficient. Pore pressure may increase (e.g., as a result of rain or snowmelt infiltration) causing the shear stress to decay and the layer to slip along its base. More elaborate models have introduced additional mechanisms — such as dilatancy (the expansion of the pores under the effect of shear), pore pressure diffusion, and rate-dependent friction μ — for providing more realistic descriptions of slope failure and flow propagation [*Iverson*, 2005; *Cassar et al.*, 2005; *Schaeffer and Iverson*, 2008; *Pailha et al.*, 2008; *Louge et al.*, 2011]. For certain saturated materials (e.g., when the fluid density matches that of the particles), granular materials can be considered suspensions of neutrally buoyant particles. Dilatancy and particle migration (depletion) away from the bed can combine to create a thin, fluid basal layer that lubricates the layer above and allows it to slip along the sloping bed. This lubrication process, sometimes referred to as *hydroplanning*, has been proposed as an explanation for the high mobility of submarine avalanches [*Elverhøi et al.*, 2005; *De Blasio*, 2011] and certain subaerial flows [*Legros*, 2002]; it is consistent with rheometric observations of model suspensions in the laboratory [*Barnes*, 1995; *Sochi*, 2011]. The main unknown factor in this approach concerns the mechanism that initiates particle depletion away from the sloping bed if the material is initially at rest.

Another approach is to consider the layer as one solid, rigid material. The simplest model is the sliding block model, in which the bottom shear stress τ_b is linked to the normal stress σ_b through a bed friction coefficient μ: $\tau_b = \mu \sigma_b$. Failure occurs if $\mu > \tan \theta$. This model suffers from the same shortcomings as the saturated, frictional Coulomb model (see above): in the absence of a mechanism describing the reduction in the friction coefficient μ, it is not very helpful. For viscous fluids, lubrication theory shows that a rigid slab can slip along a solid boundary if there is a thin layer of liquid under pressure between them [*Batchelor*, 1967]. Glaciological studies have identified at least two sliding mechanisms for glaciers which explain how liquid water can appear underneath the glacier sole [*Cuffey and Paterson*, 2010]: (i) the partial separation of the glacier base from the ground and (ii) regelation (pressure melting). In the former process, ground roughness and undulations are assumed to promote clearance between the gliding rigid snowpack and ground downhill of each bump. The resulting local cavities are filled with water, thus reducing basal friction [*Nye*, 1969]. In the latter process, the stoss sides of bumps experience higher pressure than the lee sides and locally basal temperatures reach melting point [*Weertman*, 1979].

All of these studies have been sources of inspiration for modeling gliding snow. In the following section, we will examine how these approaches have shed light on the mechanisms governing gliding snow. Although there is currently no consensus on the actual sliding mechanism, the most reasonable explanation lies in the role played by a lubrication layer and excess pore pressure at the snowpack base (see sections 3.3 and 3.4), an explanation that comes from investigations into glacier sliding and debris flow initiation. Two caveats are in order: even today, it is unclear how insightful any analogy between glaciers, debris layers, and seasonal snowpacks actually is; furthermore, glacier sliding and debris flows still stimulate vibrant debate even though they have been extensively studied over the last 50 years [*Fowler*, 2010; *Iverson*, 2003].
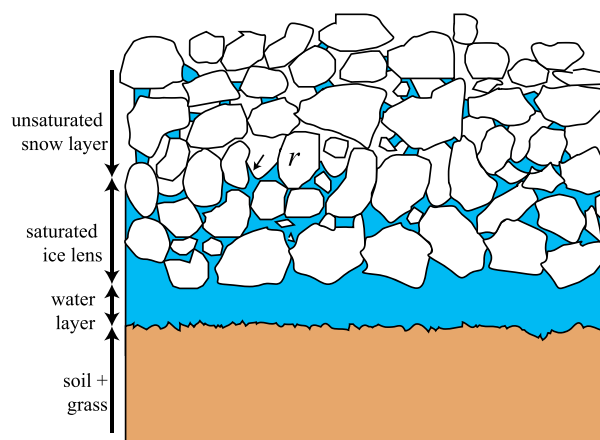
Figure 7. Sketch of a lubricating water layer within the snowpack: a thin film of water exists between the frozen ground and the base of the snow cover. The base of the snowpack is water saturated, but in the upper layer, a pendular regime takes place, in which free water percolates down to the bottom.

3.2. Earlier Work: Sliding Block Models

Haefeli [1939] performed sliding block experiments using snow samples on an inclined glass plate. He observed a significant drop in τ_b with air temperature as well as a nontrivial dependence of μ on σ_b, snow temperature, and block velocity. Theoretical considerations led *Moskalev* [1967] to suggest a linear decrease of μ as the thickness of the water-saturated layer at the base of the snow cover increases. The main shortcoming of this approach is that by focusing on the tribological characterization of μ, it provides general results which hold true for all slopes; however, glide avalanches occur under very specific conditions.

Taking the heterogeneous nature of bed contact into account, *in der Gand and Zupančič* [1965] assumed that there are wet patches at the base of the snow cover where higher liquid water contents are concentrated. In these patches, dry friction is replaced by a viscous boundary layer of thickness δ. They assumed that the resulting mean bottom shear stress is merely the sum of the viscous and Coulombic frictional contributions:

$$\tau_b = \mu\sigma_b + \frac{\eta}{\delta}u_g, \tag{1}$$

where η is the snow viscosity within the boundary layer and u_g the gliding velocity. Note that this decomposition is incorrect because if the ground surface is broken into wet and dry areas, then each contribution on the right-hand side of equation (1) has to be weighted by a coefficient reflecting the ratio of these areas to the total surface. Equation (1) leads to a gliding velocity $u_g = \rho g h \cos\theta(\tan\theta - \mu)\delta/\eta$. From observed values of δ and gliding rates, *in der Gand and Zupančič* [1965] found that depending on the (unknown) value of μ, snow viscosity η should range from 10^4 to 10^7 Pa s in accordance with other findings [*Haefeli*, 1948; *Salm*, 1967a; *Shapiro et al.*, 1997]. These values, which are 10^7 to 10^{10} higher than water viscosity, confirm that there is something amiss with this analysis or at least inconsistent with what we know about the viscosity of concentrated suspensions [*Zarraga et al.*, 2000].
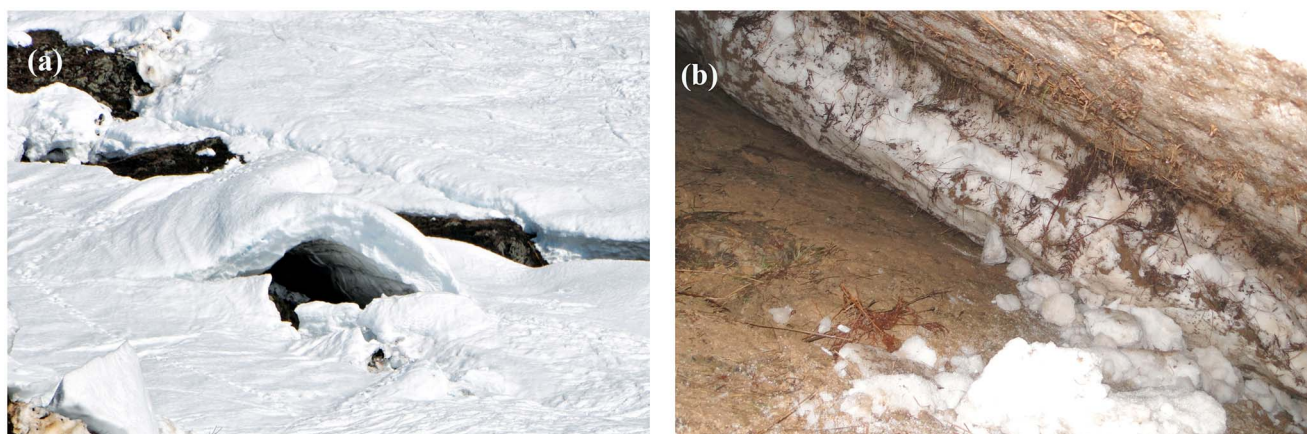

Figure 8. Field evidence of separation between the snowpack and ground: (a) undulating snow cover at Saint-François-Longchamp and (b) uplift of the slab near the damaged tower at Cauterets.

Figure 9. Typical example of a wet patch: locally, the ground surface has been leached, whereas in the surrounding area, the grassy surface is intact.

3.3. Water Layer Under Pressure

Lackinger [1986, 1988] elaborated on this approach by considering that wet patches result from the trapping of free water between the base of the snow cover and the ground, a process he referred to as "damming." He was not very explicit about the precise mechanism giving rise to this trapped water. However, let us assume that a thin layer of liquid water is trapped upstream of an obstacle, at the interface between the snowpack and ground over a length ℓ (see Figure 6b), and that the base of the snowpack is sufficiently impervious for the pressure within the layer to be hydrostatic; then, the mean normal component of the pressure force per unit width is $F_p = \frac{1}{2}\rho_w g \ell^2 \sin^2 \theta$. This pressure force counterbalances the normal component of the snowpack weight $F_n = \ell \sigma_b$ if

$$\frac{\ell}{h} = 2\frac{\rho}{\rho_w}\frac{\cos\theta}{\sin^2\theta}, \tag{2}$$

where ρ_w denotes water density. Typically, for $\rho/\rho_w = 0.4$ and $\theta = 45°$, we find $\ell/h \approx 1$, which is a reasonable value for the patch length (relative to the snow depth). Note that *Lackinger* [1986] used a stability index and additional contributions to maintain equilibrium (cohesion and Coulomb friction), but the order of magnitude of the ℓ/h ratio is the same. An interesting feature of equation (2) is that the ℓ/h ratio decreases with increasing bed inclination, which may explain why glide avalanches, although usually requiring slopes of a sufficient inclination, can on rarer occasions be observed on gentle slopes: for $\rho/\rho_w = 0.4$ and $\theta = 15°$, we find $\ell/h \approx 12$.

The cornerstone of this approach is the development of layers of water under pressure. *Lackinger* [1986] mentioned that an ice layer of a few centimeters in thickness is often observed at the base of snow cover and can be considered an impermeable boundary. Ice layers were observed at the base of the snowpack in both Saint-François-Longchamp and Cauterets (see the supporting information). Key questions concern the mechanisms by which an ice lens can be impermeable and how it is pushed up to allow the development of a lubricating layer of water, as sketched in Figure 7. One possible mechanism is evoked by *Endo* [1984]: snow cover gliding over undulating terrain may lead to partial separation when bumps lift up a sufficiently rigid snowpack base. In different places near the starting zone in Saint-François-Longchamp and in the snow deposit of Cauterets, the snow cover had been lifted up locally by natural obstacles, as shown in Figure 8. In the former case, snowpack uplift was observed from the outset of the ski season, demonstrating that snow gliding rates were high in the early season, but did not lead to avalanche release. In the latter case, the uplift occurred concomitantly with the toppling of the chairlift tower and, therefore, was more likely to have been the consequence of snow gliding than its cause.

Another mechanism is related to frost heave, whose effects are especially marked for silt-grained soils [*Matsuoka*, 1998; *Dash et al.*, 2006; *Matsuoka*, 2005; *Matsumoto et al.*, 2010]: the formation of ice lenses within soils susceptible to frost can cause a centimetric upward displacement of the ground interface and may lead to a rapid separation of the snowpack from the ground (typically within 1 day). On alpine slopes, diurnal heave can range from a few millimeters to 3 cm. Frost heaves usually occur early in the season, before the formation of a deep snow cover, but they can also occur when snow meltwater infiltrates the soil and refreezes. Note that thawing may also cause a sudden downward displacement of the ground surface, thus partial separation of the snowpack from the underlying ground [*Matsuoka*, 2005].

A closer examination of the starting zone in Saint-François-Longchamp showed that the ground surface was mostly covered with flattened grass (with no signs of strong friction, such as soil abrasion and uprooted vegetation), but as shown in Figure 9, there were also patches (typically of a few square meters) where grass was partly covered by mud deposits. These patches may be the remnants of the layer of water under pressure.

The second question involves the permeability of basal ice layers. As ice is a porous medium, one possible explanation is that surface tension at the interface between the saturated basal layer and the unsaturated snowpack (see Figure 7) impedes the upward motion of water while allowing the downward drainage of free water in a pendular regime. The pressure difference at this interface is given by the Laplace law:

$$\Delta p = 2\frac{\gamma}{r},\tag{3}$$

where γ denotes the air/water surface tension and r is the typical radius of curvature of the menisci, which is of the same order of magnitude as the mean distance δ between two ice crystals of diameter d: $\delta = d(1 - \sqrt[3]{c/c_m})$, where c is the ice volume concentration and $c_m = 0.92$ is the maximum concentration. Typically, for snows of density 600 kg m^{-3} ($c = 0.6$) and crystal diameters $d = 1$ mm, one finds $\delta = 0.1$ mm and $\Delta p = 1.1$ kPa. Laboratory experiments with dense snow samples (density ranging from 550 to 590 kg m^{-3}) in a pendular regime have given pressure jumps Δp as large as 3.8 kPa [*Colbeck*, 1974b; *Marsh*, 2005]. These values correspond to pressure heads $h_w = \Delta p/(\rho g)$ ranging from 10 cm to 40 cm, and so the lens length $\ell = h_w \sin\theta$ ranges from 15 cm to 60 cm for $\theta = 45°$. This is insufficient to support the normal load imposed by the snowpack weight. With permeability coefficients as large as 10^{-10} m^2 [*Jordan et al.*, 1999], the maximum pressure gradient at the base of the snow cover does not exceed 8.5 kPa m^{-1} [*Marsh*, 2005]. If we use the example of a 5 cm thick ice layer on top of a layer of water with a pressure head $h_w = 1$ m (to support the snow load), then the pressure gradient through the ice layer should reach 200 kPa m^{-1}; this is 20 times greater than the maximum value given by *Marsh* [2005].

To summarize, layers of water under pressure may exist at the base of the snow cover, but while they can reduce bottom shear stress significantly, the level of pressure is not sufficient to cause a complete collapse of basal shear strength. For instance, if we consider a 2 m thick snowpack with average density $\rho = 400$ kg m^{-3} undermined by a layer of water subject to a pressure head $h_w = 40$ cm, then the normal stress is $\sigma_b = \rho g h \cos\theta = 5.5$ kPa and the effective normal stress $\sigma'_b = \sigma_b - p = 1.6$ kPa, causing a 70% decrease in bottom shear stress.

3.4. Water Pressure Diffusion

Another explanation, closely related to Lackinger's theory, has been given by recent investigations into the unsteady creep and slip of dilatant soil layers: as a result of grain rearrangement (dilation/contraction phases), water pressure may be diffused through the pores of the saturated layer and alter shear strength significantly [*Iverson*, 2005; *Schaeffer and Iverson*, 2008]. In this process, pressure diffusion results from the compressibility of the granular skeleton, not from water compressibility (which is tiny). Careful laboratory experiments with highly concentrated, density-matched suspensions in inclined flumes have confirmed that fluid seepage through a granular matrix at rest is sufficient to cause the water pressure to increase significantly [*Andreini et al.*, 2013]. When water pressure is sufficient to counterbalance the stress generated by the weight of the granular matrix, the material slips along the flume bottom. Dilatancy within the basal layers leads to the diffusion of water pressure and thus an increase in the bottom shear strength, with the consequence that sliding rapidly comes to a halt. Another cycle of slippage may occur, depending on fluid seepage and material compaction. In contrast to Lackinger's theory, there is no need for an ice layer on top of a layer of water under pressure to create slip: it is the combination of fluid seepage, pore pressure diffusion, lubricated grain contacts, and dilatancy that leads to significant fluctuations of basal shear strength over time. As pointed out by *McClung* [1981], it is unlikely that water pressure alters the stress distribution in the absence of snow dilatancy in the basal layers. However, there remains a question about the possibility of a dilatant behavior of snow layers at the base of the snow cover, an issue that has not so far been documented, to the best of our knowledge. To summarize, this similarity to landslides may provide some additional physical insights into the actual mechanisms of snow sliding, but the basis for this similarity is still speculative.

3.5. Lubrication Layer

McClung [1980, 1986], *McClung and Clarke* [1987], and *McClung et al.* [1994] drew on the results obtained by *Weertman* [1979] and *Nye* [1969] to identify two sliding mechanisms for snowpack: the two main effects induced by free water are the reduction in snowpack viscosity and the partial separation of the snowpack base from the ground. *McClung* [1980, 1981] deduced that the distribution of water-filled cavities is a function of ground roughness, and by elaborating on Nye's theory and assuming that snow behaves like a compressible viscous fluid, he ended up with a linear basal friction law:
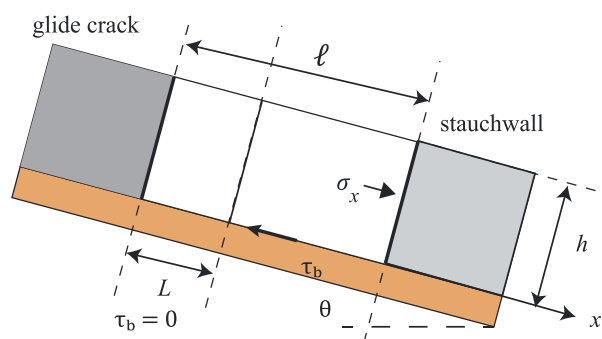
$$\tau_b = \frac{\eta}{2(1-\nu)}\frac{u_s}{D_h},\tag{4}$$

Figure 10. Slab geometry considered by *Bartelt et al.* [2012].

where η denotes the shear viscosity of snow, ν is a viscous analog of the Poisson ratio (accounting for snow compressibility), u_s represents the slip velocity, and D_h is called the stagnation depth, which is related to the statistical distribution of ground undulations. For single sinusoidal wavelengths, $D_h = \lambda(\lambda/a)^2/(8\pi^3)$, where λ and a denote the wavelength and amplitude of ground undulations, respectively [*McClung*, 1981]. The linear viscous fluid assumption is a crude one: for dense snow, rheometrical tests exhibit a nonlinear viscoelastic behavior (shear thinning, with a shear thinning index close to 1/3, as in Glen's law used for ice) [*Scapozza and Bartelt*, 2003; *Delmas*, 2013]. However, several experiments have tried to estimate bulk shear viscosity: it has usually been found that snow viscosity varies by several orders of magnitude as a function of temperature, density, and liquid water content: η ranges from 10^6 Pa s to 10^{12} Pa s [*Haefeli*, 1948; *Bucher*, 1948; *Salm*, 1967a; *Haefeli*, 1967; *Salm*, 1982; *Shapiro et al.*, 1997; *Teufelsbauer*, 2011]; the typical values for snow at $T = 0°C$ with $\rho = 400$ kg m^{-3} are $\eta \sim 5 \times 10^{10}$ Pa s and $\nu \sim 0.2$ [*Shinojima*, 1967; *Shapiro et al.*, 1997]. If we again consider a 2 m thick snowpack (with average density $\rho = 400$ kg m^{-3}) on bumpy sloping ground ($a = 10$ cm, $\lambda = 10$ m, and $\theta = 45°$), then the sliding velocity u_s calculated from equation (4) ranges from 1.2 cm h^{-1} to 3.6 m s^{-1}. Conversely, the typical slip velocity $u_s \sim 10$ cm h^{-1} observed prior to avalanche release is obtained by using a shear viscosity $\eta \sim 10^9$ Pa s. From this perspective, although poorly constrained, the numerical estimates provided by equation (4) seem realistic.

In contrast with Lackinger's theory, *McClung* [1981] and *McClung and Clarke* [1987] assumed that the water pressure was hydrostatic and emphasized that free water created cavities along the ground, lubricated contact between the ground and the base of the snow cover and/or softened the basal layer. Although the significant permeability of snow justified dismissing the water pressurization effect, this assumption conflicts with lubrication theory: for a Newtonian fluid to lubricate two adjacent mobile interfaces, fluid pressure has to increase to support the weight of the upper interface. In particular, for glaciers, subglacial water pressure has been long identified as the key to explaining glacier sliding [*Cuffey and Paterson*, 2010]. The only possibility is thus snow softening induced by a reduction of snow viscosity in the basal layers when the liquid water content is increased.

3.6. Role of the Downstream Boundary Condition

Recently, new theories have emerged to explain the release of glide avalanches; they emphasize the time evolution of the phenomenon rather than focus on the statics of stationary snow cover. The idea that the time dependence of basal resistance is a key factor in glide avalanche release is not new [*Nohguchi*, 1989],

Figure 11. View of the transition area between the starting zone and the deposit at Saint-François-Longchamp (photograph taken on 4 March 2012).

but it was not until very recently that a broader physical picture was proposed by *Bartelt et al.* [2012]. These authors considered a slab of length L (see Figure 10). Over a short length ℓ, there is a collapse of bottom shear resistance, which ends static equilibrium. In the ensuing stress redistribution, a part of the frictional force is taken up by an increase in the tensile stress in the downhill direction (denoted by σ_x). A glide (tensile) crack develops, forming the upper boundary of the slab. The stauchwall experiences a gradual increase in compressive stress. Assuming a viscoelastic behavior for snow, *Bartelt et al.* [2012] ended up with a second-order
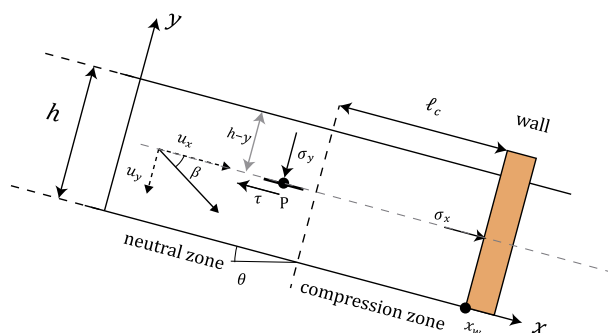
Figure 12. Definition of the neutral and compression zones.

differential equation for σ_x, whose phase portrait showed the existence of a focus point. In practice, this means that once destabilized, the slab always reaches a new equilibrium at "large" times (compared to the time associated with elastic wave propagation), but this path to equilibrium may be characterized by wide fluctuations in axial strain rates. If these strain rates exceed a critical value, then the stauchwall fails (brittle compressive failure) and the avalanche is released.

Although this model provides a compelling description of the release process, quantification is a delicate issue in the absence of rheometrical measurements of snow properties. Furthermore, it is often difficult to locate the position of the stauchwall. As shown in Figure 11 for Saint-François-Longchamp, if any stauchwall existed, it was destroyed by the subsequent avalanche. In the same picture, a transition zone is seen at the foot of the starting zone (at 2010 m above sea level, slope 22°): there was a gradual change in the avalanche path roughness over a 20 m length. In the starting zone, the avalanche slid over grassy ground, whereas in the lower part of its path it eroded the snow cover and thus slid on a snow interface. In Cauterets, no stauchwall was observed, but the snow cover there was the result of a superimposition of avalanche deposits.

4. Force Due To Gliding Snow

Modeling capabilities have dramatically improved since the first analytical calculations performed by *Haefeli* [1939] and even since more recent finite-element simulations of snowpack changes [*Bader et al.*, 1988; *Kleemayr*, 2004; *Nicot*, 2004; *Teufelsbauer*, 2011]. Yet the ability to accurately explain the interaction between a gliding snowpack and an obstacle still remains some way off.

For many years, in the absence of powerful computational resources, scientists working in snow science could only investigate simplified problems and geometries. In practice, this meant that they had to solve one-dimensional flow problems using simple constitutive equations about snow behavior and an idealized description of the interaction between snow and obstacles. Even today, with the assistance of powerful computers and numerical techniques, the overall problem remains very difficult due to the fact that snowpacks exhibit considerable spatial variability in terms of their mechanical properties and composition, depth, etc. [*Schweizer et al.*, 2008].

A further issue is that part of the accumulated knowledge on avalanches has been transcribed into the form of guidelines and has thus become somewhat intellectually "frozen." From the initial publication in 1952 to the latest update [*Margreth*, 2007a], the Swiss guidelines have always been based on more than a theoretical analysis of the interaction between creeping/gliding snowpacks and obstacles — they have also been based on practical tests and field surveys. They have slowly evolved in parallel with new findings and the experience gained from building kilometers of protection barriers. They have been criticized on several occasions because they are based on oversimplified assumptions of the actual rheological behavior of snow [*McClung*, 1993] and because, in some regions, they fail to provide correct approximations of snow forces [*Larsen et al.*, 1989; *Katakawa et al.*, 1992; *Shapiro et al.*, 1997; *Rudolf-Miklau and Sauermoser*, 2011; *Harada et al.*, 2014].

Below, we focus on the calculation of the forces exerted by snow cover of depth h on an infinitely wide frictionless wall normal to the slope bed (see Figure 12); this is the standard configuration used in most papers. The following sections summarize the main results, whereas Appendices A–C give further information about the derivation of the forces. The problem of a finite-size obstacle such as a tower is discussed in Appendix D. The models presented in this section are then compared with the data obtained for the Cauterets and Saint-François-Longchamp avalanches in section 6.

4.1. Haefeli's Approach
Even though Haefeli's work has been revisited and updated, the series of seminal papers written by *Haefeli* [1939, 1942, 1944, 1948, 1951] around 70 years ago is still viewed as the cornerstone of the Swiss guidelines

[*Margreth*, 2007a]. Due to their importance in the development of concepts still in use today, his main findings are summarized and contextualized with respect to current knowledge in Appendix A.

Haefeli considered an infinitely long uniform snowpack. The wall induces a stress and strain redistribution over a distance ℓ_c in a zone referred to as the *compression zone*. He assumed that the flow was perfectly plastic and coaxial. In other words, the snow undergoes irreversible strains without any increase in stresses, and the directions of the principal stresses and strains are coincident [*Davis and Sevladurai*, 2002]. With regard to the kinematic conditions, Haefeli assumed that the velocity profile in the far field, referred to as the *neutral zone*, was known and linear, with a slip velocity denoted by u_g. As the snowpack thickness is uniform, the shear and y normal stresses are known in advance. The wall produces a gradual deceleration of the snowpack, and thus, the force exerted by the snowpack on the wall comprises a static component (representing the plastic force in the absence of any obstacle) and a dynamic component (which results from the deceleration of snow within the compression zone), which can be seen as a corrective term to the static contribution. Reasoning with the help of Mohr's circles, Haefeli deduced the stress distribution within the compression zone.

In the end, Haefeli found that the total force is the sum of the static and gliding contributions:

$$F = \frac{1}{2}\rho g H^2 \left(\cos^3\theta(1 - 2\tan\beta_{45}) + K_h N\right),$$ (5)

where $H = h/\cos\theta$ is the snow depth measured vertically, K_h is Haefeli's creep factor, N is Haefeli's gliding factor, and β_{45} is the creep angle for a 45° slope (see Appendix A for the expressions of these coefficients). Haefeli's work has been revisited, but the structure of the final equation (5) has remained the same.

A modern interpretation of Haefeli's work raises a number of issues regarding the consistency of his treatment of the physical world. Haefeli introduced significant limitations by considerably simplifying physical representations of the real world, such as the one-dimensional nature of the problem (he did not consider a gradient in the x direction). This is, however, a strength rather than a weakness, in that it allows the main physical effect brought out in the analysis to emerge in its simplest form. Other assumptions have been more criticized. Haefeli did not consider the conservation of mass and momentum but rather assumed a velocity distribution. The only explicit hypothesis involving the rheology of snow was that it behaved like a purely plastic material, and he implicitly used the principle of coaxiality. A closer inspection of Mohr's circles, looking for stresses, shows that snow should behave like a noncohesive material, with an internal friction angle φ that depends on both the creep angle β and ground inclination θ; therefore, φ cannot be a constitutive parameter as required by plasticity theory (see Appendix A). This also conflicts with the concept of perfect plasticity used by Haefeli, which should mean that snow behaves like a cohesive frictionless material. Furthermore, the velocity field introduced by Haefeli is not consistent with an associated flow rule introduced by the coaxility principle (see Appendix A).

In Haefeli's defense, we can point out that although the concept of yield surface was established in the 1940s, plastic theory was still in a developmental phase. The concept of plastic flow dates back to contributions by von Mises and Hencky in the 1920s; Hill's theory, together with Drucker and Prager's work on plasticity, was published in the 1950s, and theoretical insights into the coupling between dilatancy and friction came from the Cambridge school (Roscoe, Schofield, Wroth) and from Rowe in the 1960s. Compared to the models developed by Campell, Pollack, and Mougin based on a static equilibrium of the snow volume retained by the wall [*Bucher*, 1948; *Roch*, 1955], Haefeli's work was clearly a breakthrough, even though subsequent findings in the field of plasticity have revealed some inconsistencies in his treatment of the stress distribution.

4.2. Bucher's Model
Bucher reformulated Haefeli's model so that snow was regarded as a compressible viscous fluid rather than a plastic material (see Appendix B). By introducing a Newtonian constitutive equation, instead of assuming the velocity, *Bucher* [1948] determined it from the momentum balance equation. To that end, he assumed that the classic no-slip condition along the bottom holds true and the static pressure term is negligible. He was then able to find an approximate solution to the velocity field in the compression zone. He considered that the total force exerted on the wall results from the viscous normal stress applied to it. There is no static component in his calculation.

Bucher [1948] found that the total normal force exerted on the wall (per unit width) is

$$F_g = -\int_0^h \sigma_x(0, y)dy = \frac{\rho g h^2 \sin\theta}{\sqrt{2(1 - \nu)}},$$ (6)
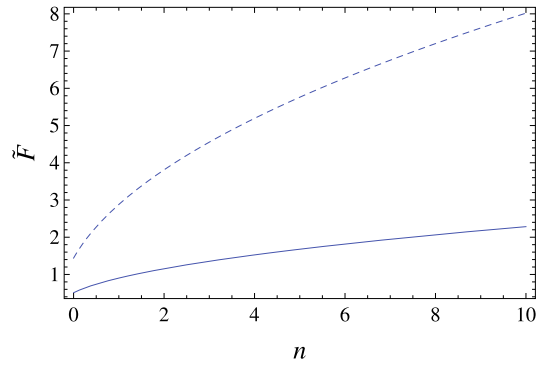
Figure 13. Variation of the scaled force $\tilde{F} = F / \left(\frac{1}{2} \rho g H^2 \right)$ as a function of the velocity ratio n ($n = (N^2 - 1)/3$; see equation (A1)) for a slope $\theta = 45°$, with $\rho = 400$ kg m^{-3} ($\nu = 0.258$). The solid line represents McClung's model (7), while the dashed line shows the scaled force computed using Swiss guidelines (9).

where ν denotes the Poisson ratio (the transverse-to-axial-strain ratio in elasticity). Although the structure of Bucher's equation (6) differs from Haefeli's gliding force (A7), their ratio gives $3 \sin(2\theta)/\sqrt{32(1 - 2\nu)} \sim 0.9$ for $\theta = \pi/4$ and $\nu = 1/3$. We conclude that in the absence of gliding, Haefeli's and Bucher's models are consistent with each other in spite of the significant differences in approach. *Salm* [1977] mentioned that some work had been done to extend Bucher's theory to gliding snowpacks, which resulted in an empirical expression in which the actual snow depth was replaced by a fictitious depth.

The absence of a static pressure term is uncertain as for compressible materials, we expect there to be a thermodynamic pressure that reflects the isotropic stress distribution in the absence of other strains. Another pressure term resulting from bulk compressibility can be added to this static pressure [*Chadwick*, 1999]. Compressible viscous fluids form the Reiner-Rivlin fluids, which are a generalization of the classic incompressible Newtonian fluids [*Coleman et al.*, 1966; *Bowen*, 1989]. In Bucher's defense, we should point out that Reiner-Rivlin fluid theory was only developed in the late 1940s, and it is likely that Bucher was unaware of these developments in continuum mechanics.

4.3. McClung's Approach

McClung [1982] used the same constitutive equation as *Bucher* [1948], i.e., a compressible viscous Newtonian law. McClung thought that the assumption of no slip at the bottom of the snowpack was unrealistic, especially for dealing with problems involving clear evidence of gliding snow; therefore, he explicitly assumed that the snow cover was slipping along its bottom. As this assumption introduced a new unknown (the slip velocity), McClung needed another assumption to close his system of governing equations. Like Haefeli, he assumed that the velocity field was linear far upstream from the wall and did not satisfy the no-slip condition at the bottom. Lastly, using the principle of momentum conservation for a control volume of length ℓ_c, he determined the variation in the mean velocity and normal force with position (see Appendix C).

Like Haefeli, he considered that the total gliding force results from dynamic and static pressure terms:

$$F_g = \frac{\rho g h^2 \cos \theta}{2} \left(2\kappa \tan \theta + \frac{\nu}{1 - \nu} \right), \tag{7}$$

with

$$\kappa = \sqrt{\frac{2}{1 - \nu} \frac{D_*}{h}} = \sqrt{\frac{12n + 3.24 + \nu}{6(1 - \nu)}} \tag{8}$$

for a frictionless wall, where D_* denotes a characteristic length (see Appendix C).

4.4. Summary

The Swiss guidelines express total force as

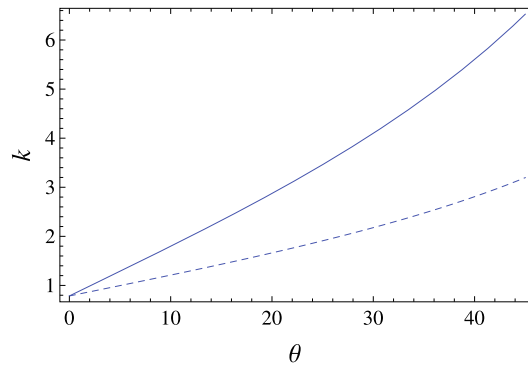$$F = \frac{1}{2} \rho g H^2 K N, \tag{9}$$

Figure 14. Variation of the ratio $k = \bar{\sigma}_x/\bar{\sigma}_y$ for McClung's model (7). The solid line represents the $N = 1.14$ ($n = 0.1$) case, while the dashed line shows the $N = 2.64$ ($n = 2$) case. Computations made for $v = 0.258$.

where $H = h/\cos\theta$ denotes snow height measured vertically, $N = \sqrt{1 + 3n}$ is Haefeli's gliding factor, and n is the velocity ratio given by equation (A1) (see Appendix A for their expression). In practice, N varies from 1.2 (rough slopes) to 3.2 (smooth slopes) [*Margreth*, 2007a]. We have also introduced the creep factor K. This can be related to Poisson's ratio using equation (B8), as introduced by *Bucher* [1948]; it has been calibrated from laboratory data:

$$K = \frac{2}{3}\cos\theta\sin\theta\sqrt{2\cot\theta\cot\beta}$$
$$= \frac{2}{3}\sin(2\theta)\sqrt{\frac{1-v}{1-2v}}$$
$$= \sin(2\theta)(2.5s^3 - 1.86s^2 + 1.06s + 0.54),$$
$$(10)$$

with s being the relative density of snow (to water). The static contribution—see equation (A6)—has been neglected as it is usually much smaller than the contribution due to gliding [*Haefeli*, 1948]. McClung's equation (7) exhibits a similar structure, but with a greater dependence on θ. The ratio of equations (7)–(9) is approximately $\frac{3}{2}\cos^2\theta$. Figure 13 compares both models using a particular case ($\theta = 45°$): other than the fact that their amplitudes differ by a factor of 3, the models show a similar dependence on n. It may seem surprising that Haefeli and McClung obtained similar results, although they were off by a multiplicative constant, since both authors took radically different approaches. However, from a dimensional analysis standpoint, given that they actually used the same variables, there was no real possibility that they could have arrived at very different results.

It is also interesting to calculate the ratio $k = \bar{\sigma}_x/\bar{\sigma}_y$. Indeed, from a mechanical point of view, there should not be much difference between avalanche forces in the limit $u \to 0$ (e.g., equation (15)) and the force exerted by gliding snow cover. McClung's model gives a stress ratio

$$k = 2\kappa\tan\theta + \frac{v}{1-v}, \quad (11)$$

where $\kappa(n, v)$ is given by equation (8). For slow wet-snow avalanches, field measurements show that much of the shear is concentrated within a basal shear layer, while the upper layers exhibit low shear rates (typically lower than 1 s^{-1}) [*Kern et al.*, 2009]. These observations lead us to choose low values of n to represent wet-snow avalanches. Figure 14 shows the variation in stress ratio k for two values of n as a function of the slope: $N = 1.1$ ($n = 0.1$) and $N = 2.6$ ($n = 2$). Typically, k ranges from 2 to 4 for a 30° slope, which is consistent with the empirical values discussed in section 5.2. According to the Swiss guidelines, however, k ranges from 4 to 8 for $\theta = 30°$.

5. Avalanche Forces

The difficulties involved in calculating the forces exerted by gliding or flowing snow are a long-standing issue [*Mougin*, 1922; *Lagotala*, 1927; *Haefeli*, 1939]—far from solved even after nearly a century of investigation. Examination of the technical literature may convince the reader that this is a confusing topic, full of conflicting statements, misconceptions, a repetition of old (and sometimes discredited) ideas, and a lack of synthesis. This comes as no surprise when even the basic terminology used to organize avalanche knowledge remains fuzzy. This problem has been faced in other fields: it took more than 150 years before a rigorous analytical treatment of viscous forces on moving bodies was proposed [*Veysey and Goldenfeld*, 2007]. For instance, it turns out that the famous Stokes result (1851) for the drag force on a sphere as a function of the Reynolds number was only correct by fortuitous accident. Resolving the experimental contradictions in the measurement of drag forces also required considerable efforts lasting decades. With regards to snow, we can now more easily understand why force calculation remains a vast fallow field of research; existing knowledge is a patchwork
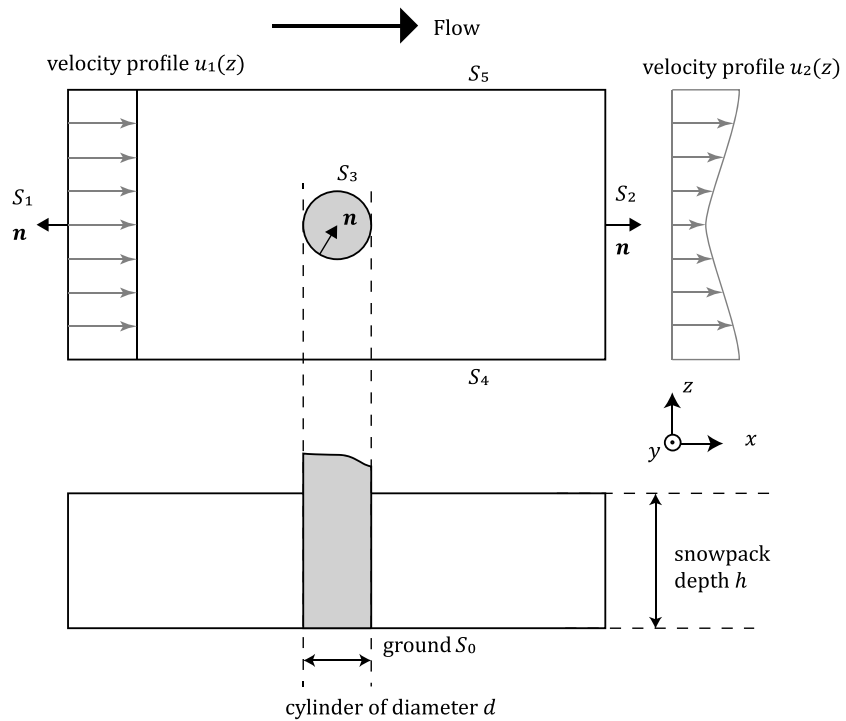
Figure 15. Volume of control surrounding a cylindrical obstacle of diameter d normal to the ground S_0. The inflow section is S_1, while the outflow section is S_2. S_3 is the interface between the snowpack and the cylinder. Each control surface is oriented by a normal vector $\boldsymbol{n}$.

combining empirical evidence and theoretical results based on similarities with other fields of research. In spite of the simplicity of the equations proposed in the various guidelines, their practical application to field studies requires considerable experience in order to avoid errors [*Roch*, 1980; *Burkard*, 1992].

5.1. Inertia- and Gravity-Dominated Regimes

The dominant historical view has been that avalanches are high-speed flows and thus their interaction with any obstacle produces forces that should depend on the kinetic energy of the flow [*Mougin*, 1922]. Yet surveys of damage caused by avalanches to different objects (houses, trains, etc.) led *Voellmy* [1955a] to distinguish between the forces due to an impact (which could be evaluated using a variant of the Bernoulli equation for compressible fluids) and the forces due the slow thrust of snow, which are assumed to be "hydrostatic." *Voellmy* [1955b] then found that the upper boundary of the avalanche pressure is

$$p_{\max} = \rho_m(gh + u^2), \tag{12}$$

where ρ_m is the snow density when encountering the obstacle, u is the (depth-averaged) velocity of the avalanche upstream of the obstacle, while h denotes its flow depth. This equation is bounded by two limiting cases: for high-speed avalanches, the maximum pressure is $p_{\max} = \rho_m u^2$, while for low-speed avalanches, the pressure scales as $\rho_m gh$. Voellmy's work initiated a host of publications on the calculation of avalanche forces, mainly focusing on the different phases of the interaction between snow and obstacles [*Salm*, 1964; *Grigorian*, 1974], the size and geometry of those obstacles [*Sommerhalder*, 1966], etc. Recent surveys can be found in *Ancey* [2006], *Gauer and Jóhannesson* [2009], *Faug* [2010], *Bovet* [2012], and *Margreth et al.* [2013]. Here we focus on the limiting case of small velocity (typically a few m s^{-1}) and small obstacles (typically a tower of diameter d).

Voellmy and subsequent authors adopted the Bernoulli equation, but the Bernoulli theorem is not easily applicable to compressible and highly dissipative fluids in complex time-dependent flows. A similar problem arises in the calculation of the front position of an intruding gravity current: von Kármán's famous result (based on the Bernoulli theorem) was correct but based on imprecise arguments. It took a couple of decades before theoreticians learned how to calculate the front position using the principle of momentum conservation in an integral form [*Huppert*, 2006].

It is essential to return to the fundamental principles of momentum conservation when calculating the forces of interaction. Using a control volume surrounding the obstacle, *Ancey* [2006] showed that once contact between the avalanche and the obstacle has been established and the flow is steady (or nearly steady), then the total force is the integral of the tensor $\boldsymbol{\phi}$:

$$\boldsymbol{\phi} = -p\mathbf{1} + \boldsymbol{\sigma}' - \rho\boldsymbol{uu}, \tag{13}$$

in which p is the generalized pressured (i.e., the sum of the pressure induced by the gravitational forces and the mean stress, also called the first invariant of the stress tensor), $\mathbf{1}$ denotes the unit tensor, $\boldsymbol{\sigma}'$ represents the deviatoric stress tensor, $\boldsymbol{u}$ is the snow avalanche velocity at the volume boundary, and ρ its density. If we take a symmetric volume of control, such as the one depicted in Figure 15, then we can deduce from the momentum balance equation for a steady flow that the force exerted on the obstacle by the moving snow is

$$\boldsymbol{F} = -\int_{S_3} (-p\mathbf{1} + \boldsymbol{\sigma}') \cdot \boldsymbol{n}\mathrm{d}S = \int_{S_0+S_1+S_2} \boldsymbol{\phi} \cdot \boldsymbol{n}\mathrm{d}S, \tag{14}$$

where the normal to the boundary of the control volume is denoted by $\boldsymbol{n}$.

In the *inertia-dominated regime*, the last term of equation (13) is dominant (it represents the flux of momentum), and the total force $F = \int_S \rho(u_2^2 - u_1^2)\mathrm{d}S$ then scales as $\rho u^2 S$, with $S = hd$ the apparent surface of the obstacle (see Figure 15). In the *gravity-dominated regime*, i.e., when velocity becomes sufficiently low, the first two parts of equation (13), $-p\mathbf{1} + \boldsymbol{\sigma}'$, play key roles. The focus of this section is given to evaluating this contribution of the noninertial terms.

Note that it is tempting to distinguish between the inertia- and gravity-dominated regimes by using a Froude number [*Mellor*, 1968, 1978; *Schaerer and Salway*, 1980], but the lack of information about the scaling of $-p\mathbf{1}+\boldsymbol{\sigma}'$ makes its introduction potentially confusing, a point already mentioned by *Salm* [1966] in the context of the propagation of free-surface waves for flowing avalanches.

5.2. Rankine's Theory

Different methods have been proposed for estimating the total normal stress $\sigma_n = (-p\mathbf{1} + \boldsymbol{\sigma}') \cdot \boldsymbol{n}$. The first one is the similarity between snow and soil. *Salm* [1967b, 1993] used Rankine's theory to relate σ_n to normal stress σ_y (in the vertical direction y):

$$\sigma_n = k\sigma_y, \tag{15}$$

with $k_{\min} \leq k \leq k_{\max}$. *Salm* [1967b] introduced the active and passive pressure coefficients:

$$k_{\max} = k_{\min}^{-1} = \tan^2\left(\frac{\pi}{4} + \frac{\varphi}{2}\right), \tag{16}$$

with φ the internal friction angle. If we assume that the normal stress σ_y is approximated by $|\sigma_y| = \rho g(h - y)\cos\theta$, then equation (15) leads to forces per unit width that resemble hydrostatic forces:

$$F = \int_0^h \sigma_n \mathrm{d}y = \frac{1}{2}k\rho gh^2 \cos\theta. \tag{17}$$

Heimgartner [1977] assumed an elastoplastic behavior for flowing snow, which led him to k having a slightly more complicated dependence on φ and τ_b. *Norem* [1990] used the passive pressure coefficient corrected by a factor accounting for sidewall effects. By back calculating the forces damaging engineered structures, *Ancey* [2006] found that k depended on the shape of the obstacle and the degree of confinement (concentration of the snow flux near the obstacle). He found that k ranged from 2 (large obstacle) to 4 (small obstacle on an open slope) or even 9 (small obstacle in a confined space).

Sovilla et al. [2010] provided high-resolution data of the pressure distribution across the flow depth for three low-speed avalanches in the Vallée de la Sionne (Switzerland). Their data lead to a factor k ranging from 5.8 to 12.5, with a mean value of 9.2. They highlighted the existence of wide fluctuations in pressure, but except for the early time points corresponding to the leading edge hitting the tower, the standard deviation was about 20% of the mean value. Given the uncertainty of the position of the free surface and snow density, and due

to the fact that snow chunks hit the sensors, these fluctuations were fairly moderate and did not put in doubt the linear increase of pressure with depth. *Baroudi et al.* [2011] and *Sovilla et al.* [2014] also found that in the field test sites of La Sionne and Col du Lautaret (France), pressure measurement depended on the sensor size (probably because small sensors and snow chunks were about the same size). *Sovilla et al.* [2014] found that snow pressure was increased by 1.7 on average when the sensor size was increased from 80 cm^2 to 1 m^2.

If we consider that the internal friction angle φ ranges from 20° (loose low-friction bulk materials such as glass beads) to 40° (high-friction coarse-grained materials), then equation (16) gives k values in the 2–4.6 range, which is consistent with the values back calculated by *Ancey* [2006], but not the field measurements in La Sionne. Elaborating on Rankine's state theory, *Baroudi et al.* [2011] explained the high k values attained as the effects of cohesion and finite size of the tower.

5.3. Hydrodynamic Approach

Another approach to estimating σ_n has been by using similarities to the drag force exerted by Newtonian fluids on obstacles of typical size d. A large body of theoretical and experimental work has led to an expression of σ_n as

$$\sigma_n = \frac{1}{2}C_d\rho u^2, \tag{18}$$

where ρ denotes the fluid density, C_d is the drag coefficient that depends on the local Reynolds number $Re = \rho u d/\eta$, η the snow dynamic viscosity, and u is the velocity in the far field (undisturbed by the obstacle). Using field measurements, a number of authors have deduced that the mean impact pressure is $\sigma_n \propto \rho v^n$, with n an index ranging from 1 to 1.7 [*Isaenko*, 1974; *Eybert-Bérard et al.*, 1978; *McClung and Schaerer*, 1985]. The key problem is that snow is not a Newtonian fluid and even if an equivalent viscosity were used, next to nothing is known about η. To provide points of reference, *Roch* [1980] suggested considering fluids whose consistency is similar to that of snow. He concluded that for flowing avalanches involving wet snow, C_d ranges from 2 to 10. For avalanche velocities in the 1–10 m s^{-1} range, *Azuar* [1980] stated that C_d varies between 1 and 3 but did not provide clear evidence. Extrapolating from results obtained for Newtonian fluids and particle suspensions, *Norem* [1990] suggested that C_d was dependent on Re via a power law: $C_d = 5.6Re^{-1/4}$. Typically, for an obstacle of width $d = 1$ m and snow with viscosity $\eta/\rho = 1$ m^2 s^2 (corresponding to melted caramel) and $u \sim 1$ m s^{-1}, the result is $C_d = 5.6$. In subsequent papers, *Norem* [1992] recommended using values of $C_d \geq 6$. The most recent field measurements at the Ryggfonn test site (Norway) have provided C_d values as high as 20–40 for slow wet-snow avalanches [*Gauer et al.*, 2007, 2008], while for the Vallée de la Sionne site, values in excess of 100 have been observed at the lowest Froude numbers [*Sovilla et al.*, 2008].

Dimensional analysis has led to the proposal that the Froude number is a natural candidate for describing flow dynamics [*Salm*, 1964; *Grigorian*, 1974; *Bozhinskiy and Losev*, 1998; *Faug et al.*, 2010] and thus the drag force has also been expressed as a function of the Froude number:

$$\sigma_n = \frac{1}{2}C_d(Fr)\rho u^2, \tag{19}$$

where the Froude number is defined using either the features of the obstacle $Fr = u/\sqrt{gH_o}$ [*Bozhinskiy and Losev*, 1998] or avalanche flow variables $Fr = u/\sqrt{gh}$ [*Sovilla et al.*, 2008; *Thibert et al.*, 2008], where H_o is obstacle height and h is avalanche depth. Physically, however, there is no clear reason why the drag coefficient should depend on the Froude number, as the interpretation of the latter deals with the flow features, not rheological behavior. Indeed, in fluid mechanics, Fr provides information on how information propagates or how flow kinetic energy compares with potential energy.

Field data obtained by *Sovilla et al.* [2008] in the Vallée de la Sionne and by *Thibert et al.* [2008, 2013] at the Col du Lautaret have shown that C_d should scale as $C_d \propto Fr^{-n}$, with n in the 1.5–2 range for wet-snow avalanches. Note that setting $n = 2$ leads to $\sigma_n = \frac{1}{2}C_d(Fr)\rho u^2 \propto \rho gh$, a scaling that is consistent with Salm's relationship (15). At the Col du Lautaret, *Thibert et al.* [2013] found that

$$C_d = 1 + 5Fr^{-2}, \tag{20}$$

giving $k \approx 5$ in equation (15). For dry-snow avalanches at the Col du Lautaret, *Thibert et al.* [2008] and *Baroudi and Thibert* [2009] obtained $C_d \propto Fr^{-n}$, with $n = 1.3$ and 1.1, respectively; this shows that for these avalanches,

the drag force exhibited velocity dependence. Although the data are not sufficiently numerous, the scaling of $C_d \propto Fr^{-2}$ seems more representative of low-velocity wet-snow avalanches.

There have been attempts to generalize Voellmy's equation (12). *Gauer et al.* [2008] proposed an empirical equation expressed as

$$p = \frac{1}{2}C_d^* \rho u^2 = \frac{1}{2}\left(C_d + \frac{f}{Fr^2}\right)\rho u^2, \tag{21}$$

where C_d is the drag coefficient (function of the Reynolds number) and C_d^* the generalized drag coefficient. *Gauer and Jóhannesson* [2009] used the empirical function determined experimentally by *Wieghardt* [1975], $f \approx 4.8\sqrt{h/d}$. *Faug* [2013] used the mass and momentum balance equations for a Coulomb friction model to justify the structure of the pressure equation (21) and to relate parameters C_d and f to the geometrical features of the flow and obstacles, as well as the grain properties.

5.4. Comparison With Gravity-Driven Flows

Experience gained in the study of related phenomena, such as landslides and debris flows, can shed light on the estimation of drag forces [*Zanuttigh and Lamberti*, 2007]. For pipeline engineering, *Zakeri* [2009] reviewed the different expressions used to calculate the pressure σ_n generated by landslides and submarine debris. Analogies with soil or non-Newtonian fluids are commonly used, and thus, equation (15) or (18) has been proposed. For debris flows involving fine- or coarse-grained sediment, both types of formulations have been proposed on the basis of field measurements, outdoor experiments with man-made slurries, or small-scale laboratory experiments: *Zhang* [1993], *Hu et al.* [2011], and *Bugnion et al.* [2012] found that the expression for hydrodynamic drag (18) (with C_d in the 3–5 range for full-scale flows) properly estimated impact pressures. A number of authors have suggested that a hydrostatic-like model (15) matched the experimental impact data well, with k estimated between 2.8 and 10, with a mean value of 4.5 [*Armanini and Scotton*, 1992; *Armanini*, 1997; *Zanuttigh and Lamberti*, 2006; *Proske et al.*, 2008].

Contrary to *Salm* [1967b], who drew on the analogy between snow and soils to justify the linearity between the normal stresses in equation (15), *Armanini* [1997] emphasized that this linearity is fortuitous and does not reflect any static effect: assuming that the front velocity scaled as $u \propto \sqrt{gh}$, as in the Ritter solution to the dam break problem, he then deduced that the dynamic pressure should vary as $\sigma_n = \rho u^2 \propto \rho g h$. Interestingly, *Roch* [1961] also showed a linear correlation between impact pressure p_i (in kPa) and height of new snow h_s (in cm), regardless of the type of avalanche: $p_i = 90h_s - 22$. As for wet-snow avalanches, $u \propto \sqrt{gh_s}$ is also a reasonable approximation of the front velocity [*Roch*, 1980], so Armanini's argument may indeed explain Roch's empirical observation.

As with avalanches, equations combining depth and velocity dependence have also been developed to reconcile the two viewpoints. Using the impact data obtained by studying small-scale saturated granular flows, *Holzinger and Hübl* [2004] adjusted the drag coefficients in equations (19) and (21). For slow flows and dense flows, they found $C_d(Fr) \approx 4Fr^{-4/3}$ and $C_d^* \approx 2.5Fr^{-1}$, respectively. Based on field data, the survey by *Arattano and Franzi* [2003] concluded that Voellmy's equation (12) was sufficient to capture the change in the force of impact.

5.5. Insights From Laboratory Experiments

Laboratory experiments have also been conducted to determine how the velocity of various fluids (including dry granular materials, granular suspensions, and viscoplastic fluids) affects drag force. In order to compare those fluids with Newtonian liquids, drag force has often been expressed as equation (18), where the drag coefficient is a function of various dimensionless numbers, such as the Knudsen number [*Boudet and Kellay*, 2010], the Hedstrom or Bingham number [*Pazwash and Robertson*, 1975; *Tabuteau et al.*, 2007], and the generalized Reynolds number [*Pfeiff and Hopfinger*, 1986; *Jossic and Magnin*, 2009].

For dense granular materials at low velocity, drag pressure is found to be weakly dependent on that velocity but to vary linearly with depth [*Wieghardt*, 1975; *Chehata et al.*, 2003]. Sustained contacts between particles carry frictional forces throughout the bulk material, and as a consequence, the stresses can be described by the empirical Coulomb friction law: for a vertical cylinder of diameter d inserted in a granular flow of depth h, the drag force is

$$\mathcal{F} = c\rho g d h^2, \tag{22}$$

where c characterizes the grain properties (surface friction and particle concentration) [*Albert et al.*, 1999; *Costantino et al.*, 2011]. The shape and size of the obstacle may slightly affect factor c and the quadratic dependence on h [*Albert et al.*, 2001]. Equation (22) is consistent with the Rankine model used by *Salm* [1967b]. A comparison of equations (17) and (22) leads to setting $c = \frac{1}{2}k\cos\theta$. For a cylinder of length L and diameter d placed horizontally at a depth h, the drag force is $\mathcal{F} = c\rho gh dL$, with $c \sim 13$ [*Guillard et al.*, 2014]. The high value of c is the result of the strong asymmetry in the pressure distribution between the stoss and lee sides of the cylinder. This cylinder is also subjected to a significantly large lift force:

$$\mathcal{L} = C_l\rho gh\frac{d^2}{4}L, \tag{23}$$

where C_l is the lift coefficient, which is a function of the diameter-to-grain-size ratio. For sufficiently large bar diameters, the lift coefficient is close to 20, which means that the lift force is 20 times higher than the buoyancy force for a liquid with the same density. This unexpected effect (compared to classic Newtonian and non-Newtonian liquids) originates from the redistribution of stresses near the moving cylinder: if we consider flows from left to right, the bottom left quadrant of the cylinder experiences very high pressures, while the top right quadrant undergoes significantly lower pressures. In the end, this anisotropic pressure distribution produces both large drag and lift forces.

The deviation from a linear pressure distribution (and thus from the quadratic dependence of $\mathcal{F}$ on h) is a likely result of confinement [*Katsuragi*, 2012]: this effect, known as Janssen's effect, occurs in confined granular flows (e.g., in a funnel or a tube) when the contact forces between grains redirect the weight toward the sidewalls, leading to an exponentially decreasing distribution of granular pressure [*Nedderman*, 1992; *Bertho et al.*, 2003; *Stone et al.*, 2004]. This may explain why *Ancey* [2006] found different values for k depending on the obstacle's degree of confinement. Note, however, that further experiments with horizontal rotating bars in a granular medium have also shown that the drag force may become independent of the depth, but contrary to the sidewall screening evoked in Janssen's effect, the pressure "shield" effect results from the anisotropic force network caused by the bar's motion [*Guillard et al.*, 2013].

The solids fraction of the granular flow affects the strength of force fluctuations: above a critical solids fraction c_c ($c_c \sim 0.603$ for glass beads with a narrow size distribution), drag force exhibits significant periodic fluctuations whose magnitude increases as the solids fraction increases [*Gravish et al.*, 2010]. These fluctuations originate from the deformation of the free surface (formation of a wedge of grains caused by the accumulation of grains in front of the obstacle) and sudden failures within the jammed region (development of shear bands) [*Gravish et al.*, 2010; *Hamm et al.*, 2011]. This may explain why *Sovilla et al.* [2010] observed significant fluctuations in the drag forces of wet-snow avalanches, especially early on when the front passed the obstacle. Indeed, in granular flows, the coarsest particles usually concentrate within the leading edge as a result of particle size segregation [*Gray and Ancey*, 2009], and this gives rise to a denser front.

At higher velocities, the pressure in shallow flows may exhibit a quadratic dependence on velocity, which is interpreted as the effect of momentum exchanges between colliding particles rather than a Bernoulli effect, as seen in fluids [*Takehara et al.*, 2010; *Boudet and Kellay*, 2010]. At very high velocities, a sharp bow shock wave and a stagnation point are generated in front of the cylinder, while a depletion region (vacuum) forms on the lee side [*Heil et al.*, 2004; *Hauksson et al.*, 2007; *Teufelsbauer et al.*, 2009; *Cui and Gray*, 2013]. For cylinders penetrating a dense granular flow, experiments show that pressure is weakly dependent on depth and velocity [*Hill et al.*, 2005; *Seguin et al.*, 2013].

Another insight brought out by the study of dense granular flows is the determination of the key dimensionless numbers. From a microstructural analysis of the change in the contact networks of granular flows in a dense frictional-collisional regime, *Ancey and Evesque* [2000] introduced the Coulomb number $Co = \rho_p a^2\dot{\gamma}/\sigma_y$, where ρ_p is the particle density, a the particle radius, $\dot{\gamma}$ the shear rate, and σ_y the vertical normal stress. They demonstrated that the bulk stresses should be a function of this number. In subsequent formulations, most authors have used the so-called *inertial number* $I = \sqrt{Co}$ and confirmed that for a certain range of flow conditions, the bulk stress tensor is controlled by this dimensionless number [*GDR-MIDI*, 2004; *Forterre and Pouliquen*, 2008]. Although the proposed scaling is essentially a phenomenological description of dense granular flows in the laboratory, and the bigger picture is still missing [*Delannay et al.*, 2007; *Börzsönyi et al.*, 2008; *Holyoake and McElwaine*, 2012; *Ancey*, 2012b], it is interesting to wonder whether this approach could shed

Table 1. Summary of the Geometric and Dynamic Features for the Case Studies[a]

Variable	Saint-François-Longchamp	Cauterets
d (m)	0.51	1.49
θ (deg)	19	35
u (m s^{-1})	0.5	10^{-4}
ρ (kg m^{-3})	500	650
H (m)	7	5
h (m)	6.6	4.1
Back calculated pressure $\bar{\sigma}_n$ (kPa)	61	200
Back calculated force $\mathcal{F}$ (kN)	205	1420
Froude number Fr	0.06	2×10^{-5}
$\hat{\sigma}_n$ given by Salm's equation (15) (kPa)	62	64
$\hat{\sigma}_n$ given by Gauer's equation (21) (kPa)	308	230
$\hat{\sigma}_n$ given by Thibert's equation (20) (kPa)	81	65
Haefeli's creep factor K (10)	0.56	0.98
Poisson's ratio ν (10)	0.258	0.394
Haefeli's glide factor N	2.4	2.4
Glide factor c (D3)	0	2
Efficiency factor η_F (D4)	1	6.5
$\mathcal{F}$ given by the Swiss guidelines (D5) (kN)	125	1966
$\mathcal{F}$ given by McClung's equation (7) (kN)	170	315
$\mathcal{F}$ given by McClung's equation weighted by η_F (kN)	170	2050

[a]We show tower dimensions, ground slope inclines, avalanche and snowpack characteristics, estimates of the forces leading to the damage observed, and the estimated total forces exerted $\mathcal{F} = \sigma_n h d = F d$ using various methods. Values for the coefficients involved in these calculations are also shown.

light on the physics of snow avalanches. For wet-snow avalanches with mean velocity u and depth h, as shear is concentrated within a shear basal layer of thickness δ [Kern et al., 2009], the mean shear rate scales as u/δ and the normal stress varies as $\sigma_y \approx \rho g h \cos \theta$. The inertial number scales as $I \propto a u/(\delta \sqrt{gh}) \propto Fr$ since the basal layer thickness is a few particle diameters ($2a$) and thus $a/\delta = O(1)$. This may explain why several field studies have found that the drag coefficient is a function of the Froude number. If this were the case, then the Froude number would just be a substitute for the inertial number.

6. Case Studies

The details of these case studies (chairlift towers damaged at Saint-François-Longchamp and Cauterets) are in the supporting information. Table 1 summarizes the features of each tower and the forces they faced:

1. The force of the avalanche which bent the second tower at Saint-François-Longchamp (diameter 51 cm, ground slope 19°) was estimated at 205 kN, i.e., an equivalent mean pressure of $\bar{\sigma}_n = 61$ kPa. The avalanche velocity was $u \sim 0.5$ m s^{-1}, its density was $\rho = 500$ kg m^{-3}, and the vertical depth of snow was approximately 7 m, leading to a Froude number of 0.06.
2. For tower P10 of the Cauterets cable car (diameter 122 cm but wider at the base; see the supporting information), back calculation from the damage observed gave values of 1420 kN of drag force (horizontal component) and 200 kPa for the depth-averaged snow pressure. Accumulated snow and avalanche deposits made up a snowpack 4.8 m deep. Its depth-averaged density was estimated at 650 kg m^{-3}. Glide velocity was estimated to average 40 cm/d before the accident but reached 4 m/d on the morning of 16 February, leading to a Froude number as low as 2×10^{-5}.

It should be remembered that these values were back calculated from an analysis of the damage; they are likely to present the lower limits of the forces and stresses rather than an accurate description of the forces exerted on the structure by the gliding mass of snow. As pointed out above, we estimate that wet-snow avalanches in their runout phase ($u \rightarrow 0$) and fast-gliding snowpacks may present similarities in terms of the forces they exert on structures. Naturally, this is a first approximation as the composition and structure

of snowpacks and wet-snow avalanches differ greatly. We assume that the main difference in the two phenomena lies in the expression of the efficiency factor introduced by Haefeli (see Appendix D): because this coefficient reflects the history-dependent growth of the compression zone, we estimate that the typical time associated with this growth is much longer than the characteristic duration of an avalanche, and so we have set $\eta_F = 1$. Furthermore, as McClung's calculations assumed an infinitely wide structure, we have calculated the force using equation (7) for an infinite width and have weighted McClung's relation (7) using Haefeli's efficiency factor (D4). This should give an estimate of the force exerted on a finite-width structure.

6.1. Saint-François-Longchamp Glide Avalanche

Salm's equation gives proper estimates of the normal stress for the Saint-François avalanche. Indeed, applying a value of $k = 4$ to equation (17), as recommended by *Ancey* [2006], gives $\hat{F} = 207$ kN and $\hat{\sigma}_n = 61$ kPa; these two values are remarkably close to the back calculations.

The drag coefficient $C_d = \sigma_n/(\frac{1}{2}\rho u^2)$ has to be close to 1000 for the Bernoulli-based estimate of pressure (18) to give a reasonably accurate value. Applying expression (20), as fitted by *Thibert et al.* [2013], gives $C_d = 1300$. This equation gives $\hat{F} = 274$ kN and $\hat{\sigma}_n = 81$ kPa, which are 30% higher than the back calculated values, but owing to the uncertainty of the back-calculation, they are quite reasonable. The empirical equation (21) developed by *Gauer et al.* [2008] gives much larger values: $\hat{\sigma}_n = 308$ kPa.

6.2. Gliding Snow at Cauterets

With regard to the models specifically developed for gliding snowpacks, Table 1 shows that both McClung's (7) and Haefeli's (D5) equations provide correct estimates as long as they are weighted using the efficiency factor η_F.

Salm's (17) and Thibert's (20) equations considerably underestimate the stress due to a gliding snowpack (by a factor of 3). Interestingly, Gauer's equation (21), which overestimates the force generated by the wet-snow avalanche at Saint-François-Longchamp, provides an estimate of the gliding stress which agrees closely with back calculations for Cauterets.

7. Concluding Remarks

In this review, we gave a broad overview of the issues related to the formation and effects of glide avalanches. The problems of snow gliding and wet-snow avalanches are closely related. While processes involving slippage of a finite volume of snow down a slope—be it the slow motion of a wet-snow avalanche or a gliding snowpack—have been studied since the very beginning of the scientific study of avalanches, in the early twentieth century, they have attracted less attention than dry-snow avalanches. The reasons are numerous. On the one hand, in terms of damage potential, they are seen as much less harmful to human activities (infrastructure, transportation, and recreational activities) than dry-snow avalanches, and thus, most research efforts have so far focused on enhancing our understanding of high-speed dry-snow avalanches. On the other hand, not all of the processes related to wet-snow lend easily themselves well to analysis [*Schweizer et al.*, 2003; *Mitterer*, 2012].

New views on the subject have come about in part not only because more research is now being done but also because global warming may shift the nature of the avalanche threat. In recent years, there has been an increase in the number of accidents caused by gliding snow and glide avalanches, especially in ski resorts, and thus there is growing concern that the very nature of the technical problems encountered in the management of high-altitude areas (such as avalanche forecasting and mitigation) has changed.

This paper aimed to emphasize the existence of a solid phenomenology of the processes related to gliding snow. Furthermore, empirical computational tools offer a zero-order description of the causes and effects of glide avalanches. The review also identified weak spots in our understanding of wet-snow behavior, some of which clearly deserve further research. The following points can be highlighted.

1. The meteorological conditions that cause snow to slip and/or form glide avalanches are well documented. The topographical features enabling snow gliding are also fairly well known. The mechanisms that govern slipping are, however, poorly understood. The most likely scenario, one that is consistent with field observations, is of the existence of wet patches of snow cover: locally, the snowpack base separates from the ground and liquid water occupies the gap. When trapped, this water can be put under pressure, which leads to a significant but local reduction of the bottom shear stress [*Lackinger*, 1986, 1988]. If the normal

stress σ_x fails to resist the resulting load, then a glide crack develops. Depending on the dynamics of this stress redistribution and the strength of the stauchwall, a glide avalanche may form [*Bartelt et al.*, 2012]. To supplement mitigation techniques based on supporting structures [*Margreth*, 2007a], the drainage of fine-grained soils could be an effective way to reduce the formation of wet patches.

2. Gliding snowpacks can generate forces on obstacles that are as large as the impact forces of high-speed avalanches. Several analytical approaches have been developed to estimate the forces on an infinitely wide obstacle. Haefeli's work especially stands out because of its insightful physical description of the problem [*Haefeli*, 1939, 1942]. Many of his developments were at the cutting edge of research at that time, and remarkably, the equation he proposed is still used today. Unfortunately, part of the equation's reasoning is flawed, but the issues related to plasticity, dilatant frictional behavior, and boundary layer theory were far from resolved in the 1930s. Subsequent developments by *McClung* [1982, 1984, 1993] corrected a number of weaknesses in Haefeli's approach, but they were still achieved within the framework of infinitely wide obstacles.

3. The crucial problem thus lies in the evaluation of the forces exerted on finite-sized obstacles. Their magnitude can be much larger than the force generated by a one-dimensional gliding snowpack. The explanation given by *Haefeli* [1939] is that a compression zone arises from the accumulation of snow upstream of obstacle, while a tensile zone also pulls the obstacle downstream. As a result, the static force generated by this combination of compressive and tensile forces substantially increases the load on a finite-sized obstacle. Introducing an efficiency factor η_F, *Haefeli* [1939, 1948] outlined a solution to this thorny problem, but in practice, this factor relies on empirical justifications rather than on a firm theoretical grounding. As shown in this paper's case studies and those presented by *Margreth* [2007b], the value of this factor is of paramount importance to a proper determination of the forces exerted, but as it varies over a wide range, its determination remains a problematic issue in engineering applications. At the end of the day, sound engineering judgment is the key to selecting a relevant value for η_F.

4. Another issue concealed within theoretical approaches and empirical methods is the great spatial variability of snow properties [*Schweizer et al.*, 2008]. Recent numerical models of changes in the snowpack are likely to overcome these limitations [*Bader et al.*, 1988; *Kleemayr*, 2004; *Nicot*, 2004; *Teufelsbauer*, 2011]. However, like many problems, there is a certain risk of using models that are very much more precise than can be justified when taking into account the random features of a snowpack and the absence of field data of sufficient accuracy. The case at Cauterets is interesting in that the snow cover surrounding the damaged tower was the result of the accumulation of snowfall and avalanche deposits. Because of the mild spells and rainfall, snow density reached incredibly high values (650 kg m^{-3} on average across the depth). Snow depth also varied considerably in the close vicinity of the tower, depending on local topography and avalanche activity over the preceding weeks. In summary, the Cauterets case is very far removed from the ideal situation addressed by theoretical models, which consider the uniform snowpacks resulting from an accumulation of snowfalls.

5. Research has focused on infinitely wide walls or small obstacles such as towers or tree trunks. For more complicated obstacles, such as wedges and deflecting walls, little is known about the effects of gliding snow. There is a clear lack of information concerning the influence of obstacle shape on the forces exerted by a glide avalanche or gliding snowpack.

6. Following the initial suggestion by *Voellmy* [1955a], we believe that the partitioning of avalanches into inertia- and gravity-driven flows offers a practical way of estimating the forces which avalanches exert on obstacles [*Ancey*, 2006]. For low-velocity avalanches (gravity-dominated regime), the forces are similar to the hydrostatic or lithostatic forces in fluids or soils at rest. For high-speed flows (inertia-dominated regime), the forces are expected to be proportional to the square of the velocity.

7. As suggested by *Salm* [1967b, 1993], Rankine's theory can be used to calculate the normal stresses for gravity-dominated flows. This leads to results that are consistent with most field data and laboratory experiments with granular flows; however, field surveys have also shown that it may fail to give the correct magnitude of forces in certain cases [*Baroudi et al.*, 2011]. Recent high-resolution field measurements have confirmed a hydrostatic-like profile for the avalanche pressure on a cylindrical tower [*Sovilla et al.*, 2008; *Baroudi et al.*, 2011; *Thibert et al.*, 2013].

8. Several formulations of avalanche force have been proposed. To be consistent with the hydrostatic-like behavior observed at low velocities, expressions based on the generalization of the drag force for Newtonian fluids must make the drag coefficient dependent on the Froude number. Theoretically, there is no strong dimensional argument supporting a dependence on a Froude number as this dimensionless num-

ber reflects the flow features rather than rheological behavior. However, from a practical point of view, this formulation may be useful as it can bridge the two limiting regimes using macroscopic flow variables (velocity and flow depth). Alternatives include the use of local dimensionless numbers, such as the inertial number used in the rheology of dense granular flows [*Forterre and Pouliquen*, 2008].

9. When looking at the table comparing model outcomes and field measurements for the case studies (see Table 1), the current analytical models seem to be reasonably satisfactory with regards to successfully computing the forces on small obstacles. It must be noted, however, that the analysis of damaged structures leads to lower bounds of the forces exerted, not an estimate of the actual forces, and so here "satisfactory" means that the models' predictions are consistent with that lower boundary. There is no possibility of discriminating between models. For instance, for Saint-François-Longchamp, Salm's equation (15) gives $\hat{\sigma}_n = 62$ kPa while Thibert's equation (20) provides $\hat{\sigma}_n = 81$ kPa. Both estimates are consistent with the back-calculated pressure value $\bar{\sigma}_n = 61$ kPa (lower bounds), but physically, we have no means of preferring one over the other.

10. Visibly, after disasters, reasons that justify damage to structures will always be found, but questions about the predictability of the magnitude of the potential forces exerted for a given period of return remain unanswered. For instance, the Cauterets cable car was designed to resist natural hazards associated with a certain probability of occurrence (period of return $T = 30$ years). Would it have been possible to anticipate a 5 m deep snowpack, snow density as high as 650 kg m^{-3}, and snow pressures in excess of 200 kPa? If the Swiss guidelines are applied thoughtlessly (i.e., without referring to the 2013 event), estimates would be of a snow depth $H = 3.8$ m (see Figure S15 in the supporting information), density $\rho = 270$ kg m^{-3}, $K = 0.7$, $c = 1.5$, and $N = 2.4$, which would lead to a total force $\mathcal{F} = 200$ kN. This is 7 times lower than the lower boundary reported in Table 1.

Appendix A: Haefeli's Approach

Here we summarize Haefeli's main findings [*Haefeli*, 1939, 1942, 1944, 1948, 1951]. The assumptions used by Haefeli were the following.

1. From a dynamic standpoint, snow cover upstream of the wall can be split into two parts: far upstream, there is a neutral zone whose stress distribution is unaffected by the wall, and adjacent to the wall, there is a compression zone in which the stress and strain distributions are markedly influenced by the wall.

2. The total force (per unit width) exerted by the snowpack on the wall can be split into two contributions: (i) a static force F_s, which is parallel to the slope and represents the total force due to the creeping plastic flow in the neutral zone on a surface normal to the sloping bed, and (ii) a gliding force F_g, which results from the deceleration of the snow within the compression zone. Guided by his intuition for physics, Haefeli did not justify this partitioning of forces. When translated into modern concepts, his treatment comes close to the perturbation techniques used to deal with boundary layers (here the boundary layer is replaced by the compression zone). Note that matched asymptotic expansions were developed after Haefeli's papers (from the 1950s onward) and were thus unknown to him at that time.

3. From the field observations he made, Haefeli kept in mind that the velocity profile was almost linear (see Figure A1). In addition, by considering snow settlement and basal slip, he assumed that this profile was entirely made up of three parameters: the creep angle (to the snowpack-free surface) β, the glide velocity u_g, and the velocity ratio

$$n = \frac{u_g}{u_s - u_g}, \tag{A1}$$

where u_g denotes the basal slip velocity and u_s the free-surface velocity. A modern treatment of this equation requires that the velocity field be determined during the calculations, but this ad hoc assumption based on observations allowed Haefeli to avoid the details of rheological law. He assumed that the flow was fully plastic throughout the neutral and compression layers, and he implicitly used the principle of coaxiality, which states that the principal axes of the stress and strain rate tensors are coincident.

4. Gliding does not influence the stress distribution within the neutral zone as it is just a steady translation of the entire snow cover; however, it profoundly modifies it within the compression zone as the basal velocity is not constant and tends to zero near the wall. The boundary velocities u_s and u_g are assumed to decrease gradually from their maximal values reached in the neutral zone to zero at the wall. As the plastic deformations gradually disappear in the vicinity of the wall, Haefeli assumed that the basal shear resistance
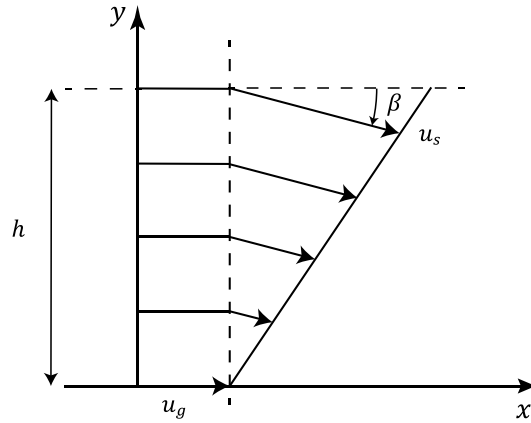
Figure A1. Shape of the velocity profile. The velocity field is assumed to take the form $u(y) = u_g + \Gamma y \cos \beta$ and $v(y) = -\Gamma y \sin \beta$ with $\Gamma = u_g/(nh)$.

decreased quadratically within the compression zone:

$$\tau_b = \tau_0 \left[1 - \left(\frac{x'}{\ell_c} \right)^2 \right], \tag{A2}$$

with $\tau_0 = \rho g h \sin \theta$ the bottom shear stress in the neutral zone and x' the distance to the wall. The resistance lost is taken up by the normal stresses $\sigma_x^{(g)}$, where the index (g) indicates that this contribution is a supplementary stress due to gliding deceleration. $\sigma_x^{(g)}$ is assumed to be uniform across the depth.

5. Even though the wall retains snow behind it, neither mass accumulation nor density variation is considered in the calculations. Likewise, snow depth does not vary with x.

Consider a point P at depth $h - y$ (see Figure 12). As the velocity field is imposed, the strain rate state is fully determined, we can thus plot the corresponding Mohr circle for strain rates, as shown by Figure A2. We deduce that the angle between the principal strain rate and the y direction is $\Lambda = \pi/4 - \beta/2$. As the snow depth is constant, we can determine the shear and normal stresses acting on a surface parallel to the ground. Using the coaxiality principle, we can then determine the position of the center C of Mohr's circle by drawing a line running from P with an angle 2Λ to the σ axis, as shown in Figure A2. As this circle is unique, the stress state on any surface facing P is determined by Mohr's circle. From Mohr's circle, we also deduce that the principal stresses are

$$\sigma_1 = \sigma_y + \tau \cot \psi, \tag{A3}$$

and

$$\sigma_2 = \sigma_y - \tau \tan \psi, \tag{A4}$$

with $\psi = \pi/4 + \beta/2$. The stress state Q on Mohr's circle gives the normal stress σ_x acting on a plane normal to the ground:

$$\sigma_x = \sigma_y - 2\tau \cot \left(\frac{\pi}{2} - \beta \right) = \sigma_y - 2\tau \tan \beta, \tag{A5}$$

from which we deduce the static force by integration over the snow depth:

$$F_s = \int_0^h \sigma_x \mathrm{d}y = \frac{1}{2} \rho g h^2 \cos \theta (1 - 2 \tan \theta \tan \beta). \tag{A6}$$

Haefeli estimated the gliding force by considering the static balance of the compression zone. Owing to the loss of basal resistance and its quadratic variation (A2), the gliding force is the difference between the downward component of weight and the basal resistance force:

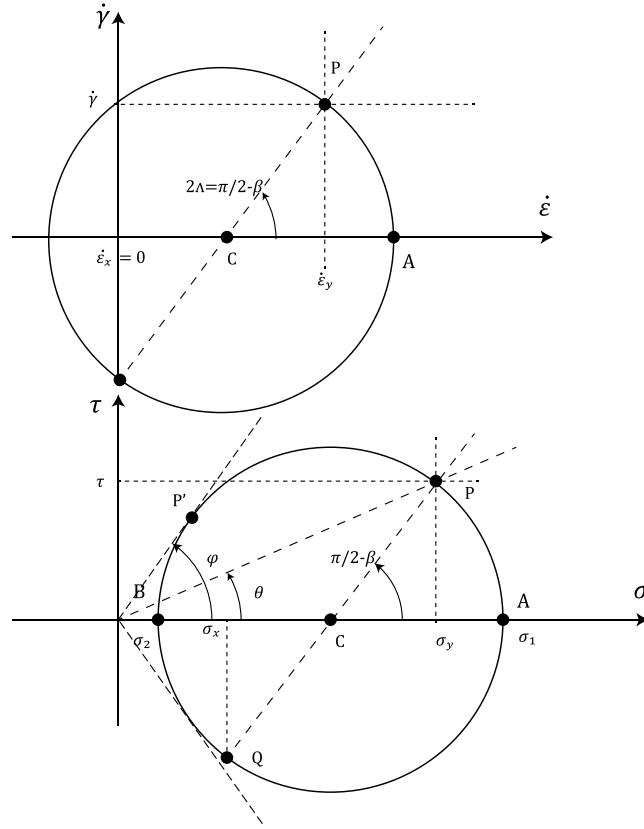$$F_g = \sigma_x^{(g)} h = \frac{1}{3} \rho g h \ell_c \sin \theta, \tag{A7}$$

Figure A2. Mohr's circles for strain rates and stresses. Here we use the sign conventions used in soil mechanics (compressive strain rates are positive) [*Nedderman*, 1992]. The normal and shear strain rates are $\dot{\epsilon}_x = -\partial_x u = 0$, $\dot{\epsilon}_y = -\partial_y v = \Gamma \sin \beta$, and $\dot{\gamma} = \frac{1}{2}(\partial_y u + \partial_x v) = \Gamma \cos \beta$ with $\Gamma = u_g/(nh)$. The circle for strain rates is easily plotted as the center C of the circle is located at $\dot{\epsilon} = \frac{1}{2}(\dot{\epsilon}_x + \dot{\epsilon}_y) = \frac{1}{2}\Gamma \sin \beta$. The point P is located at $(\dot{\epsilon}_x, \dot{\gamma}) = \Gamma(\sin \beta, \frac{1}{2} \cos \beta)$. The circle for stresses is constructed as follows. As the flow depth is uniform, the normal and shear stresses on an elementary surface parallel to the ground are $\tau = \rho g(h - y) \sin \theta$ and $\sigma_y = \rho g(h - y) \cos \theta$. Stress state P lies along the line inclined at θ to the σ axis. Because of the coaxiality principle, the angle between the normal stress axis and CP is Λ. The intersection of the Mohr circle with the σ axis gives the position of the principal axes σ_1 and σ_2, at points A and B, respectively. Mohr's circle for stresses is tangent to the straight lines $\tau = \pm\sigma \tan \varphi$ given by equation (A11). Point P' is the point of intersection between the yield criterion (A11) and Mohr's circle.

where Haefeli found the length of the compression zone to be

$$\ell_c = \frac{h}{\cos \theta} \sqrt{2 \cot \theta \cot \beta (1 + 3n)}. \tag{A8}$$

According to *Haefeli* [1942], the approximation $\tan \theta \tan \beta = \tan \beta_{45}$, where β_{45} is the creep angle for a slope $\theta = 45°$, holds true for a wide range of slopes. Experimental data provided a relationship between β_{45} and snow density ρ: $\tan \beta_{45} = 0.57(1 - \rho/\rho_i)$, where $\rho_i = 917$ kg m^{-3} is the ice density. Haefeli ended up with the following estimate of the gliding force:

$$F_g = \sigma_x^{(g)} h \approx \frac{1}{3}\rho g h^2 \tan \theta \sqrt{2 \cot \beta_{45}(1 + 3n)}. \tag{A9}$$

The total force, which is the sum of equations (A6) and (A9), can then be expressed as

$$F = \frac{1}{2}\rho g H^2 \left(\cos^3 \theta (1 - 2 \tan \beta_{45}) + K_h N\right), \tag{A10}$$

where $H = h/\cos \theta$ is the snow depth measured vertically, $K_h = \frac{1}{3} \sin(2\theta)\sqrt{2 \cot \beta_{45}}$ is Haefeli's creep factor, and $N = \sqrt{1 + 3n}$ is Haefeli's gliding factor. Haefeli's work has been revisited, but the structure of the final equation (A10) has remained the same.

A closer inspection of Mohr's circles for stresses shows that they grow in size as snow depth increases. As these circles are a one-parameter family of curves, one can show that their envelopes are two symmetric straight lines, which represent the yield surface in the $\sigma - \tau$ plane:

$$\tau = \pm \sigma \tan \varphi \quad \text{with} \quad \tan \varphi = \frac{\sin \theta}{\sqrt{\cos \beta \cos(2\theta + \beta)}}. \tag{A11}$$

Appendix B: Bucher's Model

Bucher reformulated Haefeli's model where snow was regarded as a compressible viscous fluid rather than a plastic material. By introducing a Newtonian constitutive equation, *Bucher* [1948] determined the velocity from the momentum balance equation instead of assuming it. For an isotropic compressible Newtonian fluid, the stress tensor $\boldsymbol{\sigma}$ is usually expressed as a function of the strain rate tensor $\boldsymbol{d}$, as follows:

$$\boldsymbol{\sigma} = -p\mathbf{1} + 2\eta \left(\boldsymbol{d} - \frac{\text{tr}\boldsymbol{d}}{3}\mathbf{1} \right) + \lambda \frac{\text{tr}\boldsymbol{d}}{3}\mathbf{1}, \tag{B1}$$

where $\mathbf{1}$ denotes the identity tensor. The first contribution on the right-hand side represents the pressure p, i.e., an isotropic stress independent of the rate of deformation; for compressible fluids at rest, this is often associated with the notion of thermodynamic pressure given by an equation of state. The second term is the stress generated by isochoric deformations, while the third term corresponds to the stress induced by isotropic volume variations. Two viscosities are introduced: η is the shear viscosity and λ is the compression (or bulk) viscosity [*Truesdell and Rajagopal*, 1999]. In fact, the original equation used by *Bucher* [1948] was closer to that used in mechanics of elastic bodies than in fluid mechanics. Following the developments of *Salm* [1977] and ignoring the pressure term p, we can express the strain rate tensor as a function of the stress tensor in a form reminiscent of Hooke's law:

$$\boldsymbol{d} = \frac{1}{2\eta} \left(\boldsymbol{\sigma} - \text{tr}\boldsymbol{\sigma}\frac{\nu}{1+\nu}\mathbf{1} \right), \tag{B2}$$

where ν denotes Poisson's ratio ($0 < \nu < 0.4$ for snow) [*Salm*, 1967a]. This equation is equivalent to equation (B1) when using $\lambda = 2\eta(1+\nu)/(3-6\nu)$.

Approximate solutions to the steady state on a uniform sloping bed can be found by using lubrication theory: if the gradients in the x direction are negligible relative to those in the y direction, then the velocity field $\boldsymbol{u} = (u, v, w)$ depends only on y. Density variations can be neglected, and the stress field thus satisfies

$$\sigma_x = \sigma_z = \sigma_x = \frac{\nu}{1-\nu}\sigma_y, \tag{B3}$$

$$\sigma_y = 2\eta\frac{1-\nu}{1-2\nu}v'(y) = -\rho g(h-y)\cos\theta, \tag{B4}$$

$$\tau = \eta u'(y) = \rho g(h-y)\sin\theta, \tag{B5}$$

subject to $u(0) = u_g$ and $v(0) = 0$. We then deduce the steady state solution

$$v_{ss}(y) = \frac{1-2\nu}{1-\nu}\frac{\rho g\cos\theta}{4\eta}y(2h-y), \tag{B6}$$

$$u_{ss}(y) = u_g + \frac{\rho g\sin\theta}{2\eta}y(2h-y). \tag{B7}$$

In the absence of slip ($u_g = 0$), the v/u ratio provides the creep angle [*Bucher*, 1948; *Salm*, 1977], which makes it possible to link the coefficients introduced by Haefeli with Poisson's ratio:

$$\tan\beta = \frac{v_{ss}}{u_{ss}} = \frac{1}{2}\frac{1-2\nu}{1-\nu}\cot\theta. \tag{B8}$$

The overall problem of the influence of snow cover on a retaining wall is more intricate. *Bucher* [1948] built an approximate solution by simplifying the governing equations and considering slightly different boundary conditions. He did not give many justifications for these simplifications, but we can deduce from his report that he assumed that the normal stress σ_x in the compression zone increases significantly in order to counterbalance the decrease in basal resistance. For plane deformations ($w = 0$), equation (B2) leads to the expression of the third normal stress σ_z as $\sigma_z = v(\sigma_x + \sigma_y)$. Equation (B2) leads to the following expression of the velocity gradient $\partial_x u$:

$$\dot{\epsilon}_x = \frac{\partial u}{\partial x} = \frac{1-v}{2\eta}\left(\sigma_x - \frac{v}{1-v}\sigma_y\right). \tag{B9}$$

By neglecting the normal stress σ_y, he related the normal stress σ_x directly to the velocity gradient: $\sigma_x = 2\eta\partial_x u/(1-v)$. Similarly, neglecting $\partial_x v$, he assumed that the shear stress could be approximated by $\tau = \eta\partial_y u$. As inertia is almost nonexistent, the conservation of momentum in the x direction is

$$-\rho g\sin\theta = \frac{\partial\sigma_x}{\partial x} + \frac{\partial\tau}{\partial y} \approx \frac{2\eta}{1-v}\frac{\partial^2 u}{\partial x^2} + \eta\frac{\partial^2 u}{\partial y^2}. \tag{B10}$$

For the boundary conditions, he assumed that (i) there is no slip at the bottom ($u_g = 0$); (ii) no snow penetrates into the wall ($u = 0$ at $x = x_w$); (iii) normal stress vanishes at the free surface $\partial_y u(x, h) = 0$; and (iv) in the far field ($x \to -\infty$), the velocity field matches the steady state solution (B7). Further, to make the problem tractable, he used the following approximation for the steady state velocity: $y(2h - y) \approx h^2\sin[\pi y/(2h)]$. With the change of variable $x \to \zeta x$ and $\zeta = \sqrt{(1-v)/2}$, equation (B10) is a nonhomogeneous Laplace equation that can be solved using the variable separation method. The final solution takes the form of an infinite series, for which *Bucher* [1948] provided only the first (and dominant) term:

$$u(x, y) = u_{ss}(y)\left(1 - \exp\left(\frac{\pi}{2}\zeta\frac{x - x_w}{h}\right)\right), \tag{B11}$$

with the velocity in the far field:

$$u_{ss}(y) = \frac{\rho g h^2\sin\theta}{2\eta}\sin\left(\frac{\pi}{2}\frac{y}{h}\right). \tag{B12}$$

From equations (B9) and (B12), we can deduce that the total normal force exerted on the wall (per unit width) is

$$F_g = -\int_0^h \sigma_x(0, y)\mathrm{d}y = \frac{\rho g h^2\sin\theta}{\sqrt{2(1-v)}}. \tag{B13}$$

Although the structure of Bucher's equation (6) differs from Haefeli's (A7), their ratio gives $3\sin(2\theta)/\sqrt{32(1-2v)} \sim 0.9$ for $\theta = \pi/4$ and $v = 1/3$. Furthermore, as *Salm* [1977] pointed out, the length of the compression zone (determined as the distance to the wall from which the streamwise velocity u reaches 95% of its steady state value) is

$$\ell_c = \frac{6}{\pi\zeta}h, \tag{B14}$$

and is numerically fairly close to expression (A8) found by Haefeli. We then conclude that in the absence of gliding, Haefeli's and Bucher's models are consistent with each other in spite of the significant differences in approach. *Salm* [1977] mentioned that some work had been done to extend Bucher's theory to gliding snowpacks, which resulted in an empirical expression in which the snow depth was replaced by a fictitious depth.

Appendix C: McClung's Approach

Another model for gliding snowpacks developed by *McClung* [1982, 1984, 1993], *McClung et al.* [1984], and *McClung and Larsen* [1989] was based on the following assumptions.

1. In the most general terms, creeping snow behaves like a compressible viscoelastic fluid (Burgers' fluid).
2. However, over a sufficiently long time period, elastic response can be neglected and the rheological behavior is that of a compressible Newtonian fluid, with viscosity η, Poisson's ratio ν, and density ρ. The constitutive equation is thus the same as equation (B1) considered by *Bucher* [1948]. In this respect, the contribution by McClung and coworkers can be seen as a reformulation of Bucher's model for gliding snow cover.
3. Snow glides along the ground with a slip velocity of u_g that depends on the bottom shear stress τ_b:

$$u_g = \frac{D\tau_b}{\eta}, \tag{C1}$$

where D is the stagnation depth, i.e., a fictitious depth at which the velocity profile vanishes (see also section 3.5). When the velocity profile is assumed to be linear, as in Haefeli's model, the depth ratio D/h is equivalent to the velocity ratio n introduced in (A1) by Haefeli (intercept theorem). In the absence of gliding ($u_g = 0$), bottom shear stress would be zero, but this does not hold true if the snow cover is sheared. McClung expressed the bottom shear stress as a function of $\bar{u}$ instead of the gliding velocity u_g. He thus generalized equation (C1) by introducing a characteristic length known as D_*:

$$\tau_b = \frac{\eta\bar{u}}{D_*} \text{ with } \bar{u} = \frac{1}{h}\int_0^h u\,dy, \tag{C2}$$

the depth-averaged velocity.

4. Deformation is slow and occurs mainly downward, resulting in snow compaction in the vicinity of the wall; inertia can thus be neglected. The retaining wall is frictionless.
5. In the region influenced by the wall, there is a loss of basal resistance due to snow deceleration which is taken up by the normal stress σ_x. In the direction normal to the ground, snow settlement can be neglected. The normal stress σ_y is the same as in the uniform region far upstream from the retaining wall:

$$\sigma_y = -\rho g(h - y)\cos\theta. \tag{C3}$$

Following *McClung* [1982], we consider an infinitesimal slice in the compression zone, between x and $x + dx$ (see Figure 12). In the absence of inertial terms, the force balance is

$$h(\bar{\sigma}_x(x + dx) - \bar{\sigma}_x(x)) = dx(\tau_b - \rho gh\sin\theta), \tag{C4}$$

where

$$\bar{\sigma}_x = \frac{1}{h}\int_0^h \sigma_x\,dy \tag{C5}$$

denotes the depth-averaged normal stress. Taking the depth average of the velocity gradient (B9), we obtain

$$\frac{\partial\bar{u}}{\partial x} = \frac{1 - \nu}{2\eta}\left(\bar{\sigma}_x - \frac{\nu}{1 - \nu}\bar{\sigma}_y\right), \tag{C6}$$

where $\bar{\sigma}_y$ is calculated by taking the average of the normal stress (C3). Taking the limit $dx \to 0$ of equation (C4) and making use of equations (C2) and (C6), we end up with a second-order differential equation for $\bar{u}$:

$$-\frac{2\eta}{1 - \nu}h\frac{d^2\bar{u}}{dx^2} + \eta\frac{\bar{u}}{D_*} = \rho gh\sin\theta, \tag{C7}$$

subject to the boundary conditions $\bar{u}(x_w) = 0$ and $\bar{u} \to \bar{u}_{ss} = \rho ghD_*\sin\theta/\eta$ when $x \to -\infty$. The solution is then

$$\bar{u} = \bar{u}_{ss}\left(1 - \exp^{mx'}\right) \text{ with } m = \sqrt{\frac{1 - \nu}{2hD_*}}, \tag{C8}$$

with $x' = x - x_w$ being the distance to the wall. The length of the compression zone is approximated by

$$\ell_c = 3h\sqrt{\frac{2}{1-\nu}\frac{D_*}{h}}. \tag{C9}$$

Numerical applications show that ℓ_c is proportional to the flow depth and its value agrees well with those found by Haefeli (A8) and Bucher (B14). Using equations (C6) and (C3), we then deduce that the force (per unit width) exerted on the wall by the snow cover $F_g = -h\bar{\sigma}_x$ is the sum of two contributions which *McClung* [1982] calls the dynamic and static pressure terms:

$$F_g = \frac{\rho g h^2 \cos\theta}{2}\left(2\kappa\tan\theta + \frac{\nu}{1-\nu}\right), \tag{C10}$$

with

$$\kappa = \sqrt{\frac{2}{1-\nu}\frac{D_*}{h}} = \sqrt{\frac{12n + 3.24 + \nu}{6(1-\nu)}} \tag{C11}$$

for a frictionless wall.

Appendix D: Finite-Size Effect

Most analytical models of snow force calculation have considered infinitely wide retaining walls so that the study of snow motion can be restricted to the $x - y$ plane. Yet on many if not most occasions, obstacles are of finite dimensions; i.e., their width is comparable to the snow depth. *Haefeli* [1942, 1948] tackled the problem of flow past single obstacles by running experiments in the laboratory using highly viscous materials (gelatine) and snow samples. He also monitored the force exerted by a snow cover on a metallic frame placed normal to the ground on an open slope at Weissfluhjoch. He summarized his observations by proposing a phenomenological description of the interaction between a single obstacle and a gliding/creeping snowpack (see Figure D1).

Compared to the usual case involving an incompressible Newtonian flow past a cylinder, snow compressibility and cohesion give rise to specific behaviors: over time, an accumulation zone (*Staubereich*) grows in size upstream of the obstacle, as long as the snow cover experiences creep and glide. That growth can also be enhanced as a result of snow compaction and cohesion. This accumulation zone undergoes significant compression. Downstream of the obstacle, there is a region dominated by large tensile stresses, while on either
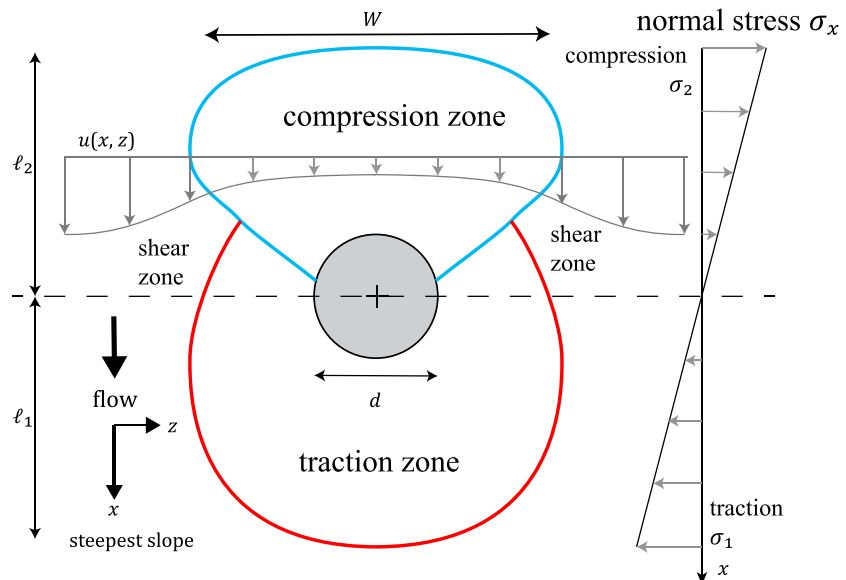

Figure D1. Sketch showing the different flow zones around a cylindrical obstacle. Adapted from *Haefeli* [1939].

side of the obstacle, shear is produced by differences in velocity. Figure D1 shows how the space surrounding the obstacle is partitioned into compression, traction, and shear zones. The snow's characteristics (density and cohesion) also vary spatially depending on the stress state. The changes in this system are history dependent, which makes the calculation of forces over control volume quite different from the case involving simple fluids shown in Figure 15.

Haefeli [1939] considered that the axial strain ϵ_{xx} (in the x direction) was related to the tensile/compressive stress σ_x by $\epsilon_{xx} = a_i\sigma_x$, where a_i denotes a compliance coefficient and $i = 1, 2$ an index referring to tensile and compressive stresses, respectively. He assumed a linear distribution of the normal stress in the transition zone (comprising the compression and tensile regions; see Figure D1): $\sigma_x = \pm\sigma_i x/\ell_i$, where σ_i denotes the stress at the boundary of the traction/compression region. Since the total tensile strain $\Delta\ell_1 = \int_0^{\ell_1} \epsilon_{xx}\mathrm{d}x$ should counterbalance the total compressive strain $\Delta\ell_2 = \int_0^{\ell_2} \epsilon_{xx}\mathrm{d}x$, then the lengths of the compression and traction zones ℓ_2 and ℓ_1 are related to each other by

$$|\Delta\ell_1| = \frac{1}{2}a_1\ell_1^2 = \frac{1}{2}a_2\ell_2^2, \tag{D1}$$

from which he deduced

$$\sqrt{\frac{a_2}{a_1}} = \frac{\ell_1}{\ell_2} = \frac{\sigma_2}{\sigma_1} = s. \tag{D2}$$

Haefeli [1939, 1951] approximated the total force $\mathcal{F}$ on the structure as the sum of the traction and compression stresses integrated over an effective surface Wh, where W denotes the typical width of the compression zone:

$$\mathcal{F} = Wh(\sigma_2 + \sigma_1) = \eta_F\sigma_2\mathrm{d}h, \tag{D3}$$

where η_F has been called the *efficiency factor* and has been empirically linked to the depth-to-diameter ratio:

$$\eta_F = (1 + \sqrt{s})\frac{W}{h} \approx 1 + c\frac{h}{d}, \tag{D4}$$

where c is an empirical gliding factor that ranges from 0.6 (low gliding rate) to 6 (high gliding rate) [*Margreth*, 2007b]. This also means that the width of the compression zone varies as $W \propto h^2/d + d$. Thus, within the limits of wide obstacles $d \gg h$ we retrieve $W \propto d$, while within the limits of small obstacles, $W \propto h^2/d$, which is in accordance with field observations that narrow elements such as cables undergo high pressures. The standard value $c = 1$ gives η_F values close to 4 for snow depths ranging from 2.5 to 3 m, and striking a 1 m wide wall, and this is in agreement with the field measurements reported by *Haefeli* [1951]. According to the Swiss guidelines [*Margreth*, 2007a], the force per unit width $F = \sigma_2 h$ can be computed using equation (9). In the end, the total force is

$$\mathcal{F} = \frac{1}{2}\eta_F\rho gH^2\mathrm{d}KN. \tag{D5}$$

More recently, *Bader et al.* [1988] have used finite-element numerical methods to solve Bucher's governing equations for a steady, uniform flow past a cylinder normal to the ground and in the absence of gliding. The constitutive equation is given by equation (B2). Their numerical results for $\nu = 0.33$ (loose snow) can be summarized by the following relationship:

$$\mathcal{F} = \rho gh^3 \sin\theta \left(0.85 + 2.68\frac{d}{h} - 0.14\frac{d^2}{h^2}\right). \tag{D6}$$

Notation

a coefficient.

c constant.

c particle volume concentration (solids fraction).

c_m maximum solids fraction.

c_c critical solids fraction.

C_d drag coefficient.

C_d^* generalized drag coefficient.

C_l lift coefficient.

d diameter.

D stagnation depth.

D_* generalized stagnation depth.

$\boldsymbol{d}$ strain rate tensor.

f friction factor.

F force per unit width.

$\mathcal{F}$ total force.

Fr Froude number.

g gravity acceleration.

h snow depth (normal to the ground).

h_s height of new snow.

h_w pressure head.

H snow height (measured vertically).

k stress ratio.

K Haefeli's creep factor.

ℓ length of the patch.

ℓ_c length of the compression zone.

L length of the slab.

L length of the obstacle.

n Haefeli's velocity ratio.

N Haefeli's glide factor.

$\boldsymbol{n}$ normal unit vector.

p pressure, first invariant of the stress tensor.

P precipitation quantile.

r meniscus radius.

Re Reynolds number.

s snow relative density.

s stress ratio.

S_w liquid saturation.

$\mathcal{S}$ surface of control.

u velocity in the x direction.

u mean velocity of the avalanche.

$\boldsymbol{u}$ elocity field.

$\bar{u}$ depth-averaged velocity.

u_g glide velocity.

u_s free-surface velocity.

u_{ss} steady state velocity.

x_w wall position.

W width of the compression zone.

W liquid water content.

β creep angle.

δ thickness of a thin layer.

$\dot{\epsilon}_x$ strain rate in the x direction.

η shear viscosity.

η_F Haefeli's efficiency factor.

γ water surface tension.

$\dot{\gamma}$ shear rate.

Γ shear rate.

κ dimensionless number in McClung's model.

Λ angle in Mohr's circle.

λ bulk viscosity.

μ friction coefficient.

ν Poisson's ratio.

φ Coulomb's angle of friction.

$\boldsymbol{\phi}$ generalized stress tensor.

ϕ_s snow porosity.

ρ snow density.

ρ_w water density.

ρ_i ice density.

σ_b stress normal to the ground.

σ_b' effective bottom normal stress.

σ_n stress normal to the obstacle.

σ_x normal stress in the x direction.

σ_y normal stress in the y direction.

σ_z normal stress in the z direction.

σ_1 first principal stress.

σ_2 second principal stress.

$\boldsymbol{\sigma}'$ extra stress tensor.

τ shear stress.

τ_b bottom shear stress.

τ_0 bottom shear stress in the neutral zone.

θ ground slope.

References

Adam, J. C., A. F. Hamlet, and D. P. Lettenmaier (2009), Implications of global climate change for snowmelt hydrology in the twenty-first century, *Hydrol. Process.*, *23*, 962–972.

Albert, I., J. Sample, A. Morss, S. Rajagopalan, A.-L. Barabási, and P. Schiffer (2001), Granular drag on a discrete object: Shape effects on jamming, *Phys. Rev. E*, *64*, 61303, doi:10.1103/PhysRevE.64.061303.

Albert, R., M. A. Pfeifer, A. L. Barabási, and P. Schiffer (1999), Slow drag in a granular medium, *Phys. Rev. Lett.*, *82*, 205–208.

Allix, A. (1925), Les avalanches, *Rev. Geog. Alpine*, *13*, 359–419.

Ammann, W. J. (Ed.) (2000), *Der Lawinenwinter*, vol. 1999, Eidgenössisches Institut für Schnee- und Lawinenforschung, Davos, Switzerland.

Ancey, C. (Ed.) (1996), *Guide Neige et Avalanches: Connaissances, Pratiques, Sécurité*, Édisud, Aix-en-Provence, France.

Ancey, C. (2005), Monte Carlo calibration of avalanches described as Coulomb fluid flows, *Philos. Trans. R. Soc. London, Ser. A*, *363*, 1529–1550.

Ancey, C. (2006), Calcul des pressions, in *Dynamique des Avalanches*, edited by C. Ancey, Presses Polytechniques Universitaires Romandes – Cemagref Editions, Lausanne, Switzerland.

Ancey, C. (2007), Plasticity and geophysical flows: A review, *J. Non-Newtonian Fluid Mech.*, *142*, 4–35.

Ancey, C. (2012a), Are there "dragon-kings" events (i.e. genuine outliers) among extreme avalanches?, *Eur. Phys. J. Spec. Top.*, *205*, 117–129.

Ancey, C. (2012b), Gravity flow on steep slope, in *Buoyancy Driven Flows*, edited by E. Chassignet, C. Cenedese, and J. Verron, pp. 372–432, Cambridge Univ. Press, New York.

Ancey, C. (2015), Avalanches, in *Oxford Research Encyclopedia of Natural Hazards*, edited by A. Graubard, Oxford Univ. Press, Oxford, U. K.

Ancey, C., and P. Evesque (2000), Frictional-collisional regime for granular suspension flows down an inclined channel, *Phys. Rev. E*, *62*, 8349–8360.

Ancey, C., and M. Meunier (2004), Estimating bulk rheological properties of flowing snow avalanches from field data, *J. Geophys. Res.*, *109*, F01004, doi:10.1029/2003JF000036.

Andreini, N., C. Ancey, and G. Epely-Chauvin (2013), Granular suspensions: II. Plastic regime, *Phys. Fluids*, *25*, 33,302, doi:10.1063/1.4793720.

Arattano, M., and L. Franzi (2003), On the evaluation of debris flows dynamics by means of mathematical models, *Natl. Hazard Earth. Syst. Sci.*, *3*, 539–544.

Armanini, A. (1997), On the dynamic impact of debris flows, in *Recent Development on Debris Flows*, vol. 64, edited by A. Armanini and M. Michiue, pp. 208–226, Lecture Notes in Earth Sciences, Springer, Berlin.

Armanini, A., and P. Scotton (1992), Experimental analysis on the dynamic impact of a debris flows on structures, in *International Congress Interpraevent: Protection of Habitat From Floods, Debris Flows and Avalanches*, vol. 6, pp. 107–116, Bern, Switzerland.

Azuar, J. J. (1980), *Avalanches, Localisation et Protection*, Centre d'Études Techniques de l'Équipement, Aix-en-Provence, France.

Bader, H. P., B. Salm, and H. Gubler (1988), Distributions of stresses and strain-rates in snowpacks, in *Sixth International Conference on Numerical Methods in Geomechanics*, vol. 4, edited by G. Swoboda, pp. 2257–2263, Balkema, Innsbruck, Austria.

Baggi, S., and J. Schweizer (2009), Characteristics of wet-snow avalanche activity: 20 years of observations from a high alpine valley (Dischma, Switzerland), *Nat. Hazard*, *50*, 97–108.

Bardou, E., P. Boivin, and H. R. Pfeifer (2007), Properties of debris flow deposits and source materials compared: Implications for debris flow characterization, *Sedimentology*, *54*, 469–480.

Barnes, H. A. (1995), A review of the slip (wall depletion) of polymer solutions, emulsions and particle suspensions in viscometers: Its cause, character, and cure, *J. Non-Newtonian Fluid Mech.*, *56*, 221–251.

Barnes, H. A. (1999), The yield stress—A review or "$\pi\alpha\nu\tau\alpha\rho\epsilon\iota$"—everything flows?, *J. Non-Newtonian Fluid Mech.*, *81*, 213–217.

Baroudi, D., and E. Thibert (2009), An instrumented structure to measure avalanche impact pressure: Error analysis from Monte Carlo simulations, *Cold Reg. Sci. Technol.*, *59*, 242–250.

Baroudi, D., B. Sovilla, and E. Thibert (2011), Effects of flow regime and sensor geometry on snow avalanche impact-pressure measurements, *J. Glaciol.*, *57*, 277–288.

Bartelt, P., T. Feistl, Y. Buehler, and O. Buser (2012), Overcoming the stauchwall: Viscoelastic stress redistribution and the start of full-depth gliding snow avalanches, *Geophys. Res. Lett.*, *39*, L16501, doi:10.1029/2012GL052479.

Batchelor, G. K. (1967), *An Introduction to Fluid Dynamics*, Cambridge Univ. Press, Cambridge, U. K.

Bebi, P., D. Kulakowski, and C. Rixen (2009), Snow avalanche disturbances in forest ecosystems—State of research and implications for management, *For. Ecol. Manage.*, *257*, 1883–1892.

Beniston, M. (2003), Climatic change in mountain regions: A review of possible impacts, *Clim. Change*, *59*, 5–31.

Bertho, Y., F. Giorgiutti-Dauphiné, and J. P. Hulin (2003), Dynamical Janssen effect on granular packing with moving walls, *Phys. Rev. Lett.*, *90*, 144,301.

Börzsönyi, T., T. C. Halsey, and R. E. Ecke (2008), Avalanche dynamics on a rough inclined plane, *Phys. Rev. E*, *78*, 11,306.

Boudet, J. F., and H. Kellay (2010), Drag coefficient for a circular obstacle in a quasi-two-dimensional dilute supersonic granular flow, *Phys. Rev. Lett.*, *105*, 104,501.

Bovet, E. (2012), Mechanics of snow avalanches and interaction with structures, PhD thesis, Politecnico di Torino, Torino, Italy.

Bowen, R. M. (1989), *Introduction to Continuum Mechanics for Engineers, Mathematical Concepts and Methods in Science and Engineering*, Plenum Press, New York.

Bozhinskiy, N., and K. S. Losev (1998), *The Fundamentals of Avalanche Science*, Eidgenssisches Institut für Schnee- und Lawinenforschung, Davos, Switzerland.

Brun, E. (1989), Investigation on wet-snow metamorphism in respect of liquid-water content, *Ann. Glaciol.*, *13*, 22–26.

Bucher, E. (1948), Beitrag zu den theoretischen Grundlagen des Lawinenverbaus, PhD Thesis, ETHZ, Zürich, Switzerland.

Bugnion, L., B. W. McArdell, P. Bartelt, and C. Wendeler (2012), Measurements of hillslope debris flow impact pressure on obstacles, *Landslides*, *9*, 179–187.

Burkard, A. (1992), Erfahrung mit der Lawinenzonung in der Schweiz, in *Internationales Symposon Interpraevent*, vol. 2, pp. 386–407, Interpraevent, Bern, Switzerland.

Caduff, R., A. Wiesmann, Y. Bühler, and C. Pielmeier (2015), Continuous monitoring of snowpack displacement at high spatial and temporal resolution with terrestrial radar interferometry, *Geophys. Res. Lett.*, *42*, 813–820, doi:10.1002/2014GL062442.

Campagne, M. (1905), *Les travaux de défense contre les avalanches dans la vallée de Barèges*, Imprimerie Nationale, Paris.

Cassar, C., M. Nicolas, and O. Pouliquen (2005), Submarine granular flows down inclined planes, *Phys. Fluids*, *17*, 103,301.

Castebrunet, H., N. Eckert, and G. Giraud (2012), Snow and weather climatic control on snow avalanche occurrence fluctuations over 50 yr in the French Alps, *Clim. Past*, *8*, 855–875.

Castebrunet, H., N. Eckert, G. Giraud, Y. Durand, and S. Morin (2014), Projected changes of snow conditions and avalanche activity in a warming climate: The French Alps over the 2020–2050 and 2070–2100 periods, *Cryosphere*, *8*, 1673–1697.

Chadwick, P. (1999), *Continuum Mechanics: Precise Theory and Problems*, Dover, Mineola.

Chehata, D., R. Zenit, and C. R. Wassgren (2003), Dense granular flow around an immersed cylinder, *Phys. Fluids*, *15*, 1622–1631.

Clarke, J., and D. M. McClung (1999), Full-depth avalanche occurrences caused by snow gliding, Coquihalla, British Columbia, Canada, *J. Glaciol.*, *45*, 539–546.

Coaz, J. W. (1881), *Die Lawinen der Schweizer Alpen*, Schmid-Franke, Bern, Switzerland.

Colbeck, S. C. (1974a), Water flow through snow overlying an impermeable boundary, *Water Resour. Res.*, *10*, 119–123, doi:10.1029/WR010i001p00119.

Colbeck, S. C. (1974b), The capillary effects on water percolation in homogeneous snow, *J. Glaciol.*, *13*, 85–97.

Colbeck, S. C. (1986), A review of the metamorphism and classification of seasonal snow cover, in *Avalanche Formation, Movement and Effects*, edited by H. Gubler and B. Salm, pp. 3–34, IAHS Publication No. 162, 1987, Davos, Wallingford, Oxfordshire, U. K.

Coleman, B. D., H. Markowitz, and W. Noll (1966), *Viscometric Flows of Non-Newtonian Fluids, Springer Tracts in Natural Philosophy*, vol. 5, Springer, Berlin.

Costantino, D. J., J. Bartell, K. Scheidler, and P. Schiffer (2011), Low-velocity granular drag in reduced gravity, *Phys. Rev. E*, *83*, 11,305.

Cuffey, K. M., and W. S. B. Paterson (2010), *The Physics of Glaciers*, Elsevier, Amsterdam.

Cui, X., and J. M. N. T. Gray (2013), Gravity-driven granular free-surface flow around a circular cylinder, *J. Fluid Mech.*, *720*, 314–337.

Dash, J. G., A. W. Rempel, and J. S. Wettlaufer (2006), The physics of premelted ice and its geophysical consequences, *Rev. Mod. Phys.*, *78*, 695–741.

Davis, R. O., and A. P. S. Sevladurai (2002), *Plasticity and Geomechanics*, Cambridge Univ. Press, Cambridge, U. K.

De Blasio, F. V. (2011), *Introduction to the Physics of Landslides*, Springer, Berlin.

de Quervain, R. (1965), On avalanche classification: A further contribution, in *Program Commissions of Snow and Glaciers International Association of Scientific Hydrology*, pp. 410–417, IAHS Publ. 69, Davos, Switzerland.

de Quervain, R. (Ed.) (1981), Unesco, Paris.

Delannay, R., M. Louge, P. Richard, N. Taberlet, and A. Valance (2007), Towards a theoretical picture of dense granular flows down inclines, *Nat. Mater.*, *6*, 99–108.

Delmas, L. (2013), Influence of snow type and temperature on snow viscosity, *J. Glaciol.*, *59*, 87–92.

Denoth, A. (1982), The pendular-funicular liquid transition and snow metamorphism, *J. Glaciol.*, *28*, 357–364.

Dreier, L., C. Mitterer, S. Feick, and S. Harvey (2013), The influence of weather on glide-snow avalanches, in *International Snow Science Workshop*, edited by F. Naaim-Bouvet, Y. Durand, and R. Lambert, pp. 247–252, ANEMA, IRSTEA, Grenoble, France.

Eckert, N., E. Parent, R. Kies, and H. Baya (2010a), A spatio-temporal modelling framework for assessing the fluctuations of avalanche occurrence resulting from climate change: Application to 60 years of data in the northern French Alps, *Clim. Change*, *101*, 515–553.

Eckert, N., H. Baya, and M. Deschâtres (2010b), Assessing the response of snow avalanche runout altitudes to climate fluctuations using hierarchical modeling: Application to 61 winters of data in France, *J. Clim.*, *23*, 3157–3180.

Elverhøi, A., D. Issler, F. V. De Blasio, T. Ilstad, C. B. Harbitz, and P. Gauer (2005), Emerging insights into the dynamics of submarine debris flows, *Nat. Hazard Earth. Sys. Sci.*, *5*, 633–648.

Endo, Y. (1984), Glide processes of a snow cover as a release mechanism of an avalanche on a slope covered with bamboo bushes, *Inst. Low Temp. Sci.*, *A32*, 39–68.

Eybert-Bérard, A., P. Perroud, G. Brugnot, R. Mura, and L. Rey (1978), Mesures dynamiques dans l'avalanche—Résultats expérimentaux du col du Lautaret (1972-1978), in *2nde Rencontre Internationale sur la Neige et les Avalanches*, pp. 203–224, Société Hydrotechnique de France, Paris. [Available at http://www.shf-hydro.org/accueil-1.html.]

Fankhauser, F. (1920), Der Lawinenverbau mittels Terrassen, *Schweizer. Z. Forstwesen*, *71*, 216–230.

Faug, T. (2010), Les récents progrès dans l'étude de la dynamique des avalanches de neige, des effets des obstacles et de la pression d'impact, in *Neige, Paravalanches et Constructions*, edited by F. Nicot and A. Limam, pp. 69–112, Lavoisier, Paris.

Faug, T. (2013), Granular force on objects and correlation length: Drag coefficient enhancement in low Froude number flow regimes, in *Powders and Grains*, vol. 1542, edited by A. Yu et al., pp. 617–621, Am. Inst. of Phys., Sydney, Australia.

Faug, T., B. Chanut, R. Beguin, M. Naaim, E. Thibert, and D. Baroudi (2010), A simple analytical model for pressure on obstacles induced by snow avalanches, *Ann. Glaciol.*, *51*, 1–8.

Feistl, T., P. Bebi, L. Dreier, M. Hanewinkel, and P. Bartelt (2014), Quantification of basal friction for technical and silvicultural glide-snow avalanche mitigation measures, *Nat. Hazard Earth. Syst. Sci.*, *14*, 2921–2931.

Forterre, Y., and O. Pouliquen (2008), Flows of dense granular media, *Annu. Rev. Fluid Mech.*, *40*, 1–24.

Fowler, A. C. (2010), Weertman, Lliboutry and the development of sliding theory, *J. Glaciol.*, *56*, 965–972.

Frutiger, H., and J. Kuster (1967), Über das Gleiten und Kriechen der Schneedecke in Lawinenverbauungen, *Schweizer. Z. Forstwesen*, *118*, 633–643.

Gauer, P., and T. Jóhannesson (2009), Loads on masts and narrow obstacles, in *The Design of Avalanche Protection Dams: Recent Practical and Theoretical Developments*, edited by T. Jóhannesson et al., pp. 95–108, European Commission-Directorate General for Research, Brussels.

Gauer, P., D. Issler, K. Lied, K. Kristensen, H. Iwe, E. Lied, L. Rammer, and H. Schreiber (2007), On full-scale avalanche measurements at the Ryggfonn test site, Norway, *Cold Reg. Sci. Technol.*, *49*, 39–53.

Gauer, P., K. Lied, and K. Kristensen (2008), On avalanche measurements at the Norwegian full-scale test-site Ryggfonn, *Cold Reg. Sci. Technol.*, *51*, 138–155.

GDR-MIDI (2004), On dense granular flows, *Eur. Phys. J. E*, *14*, 341–365.

Gex, F. (1923), Les avalanches de l'hiver 1922–1923 dans les Alpes françaises du Nord, *Rev. Geogr. Alpine*, *11*, 487–512.

Gravish, N., P. B. Umbanhowar, and D. I. Goldman (2010), Force and flow transition in plowed granular media, *Phys. Rev. Lett.*, *105*, 128,301, doi:10.1103/PhysRevLett.105.128301.

Gray, J. M. N. T., and C. Ancey (2009), Segregation, recirculation and deposition at coarse particles near two-dimensional avalanche fronts, *J. Fluid Mech.*, *629*, 387–423.

Grigorian, S. S. (1974), Mechanics of snow avalanches, in *Mécanique de la Neige*, pp. 355–368, Publication No. 114, 1975, International Assoc. of Hydrol. Sci., Grindelwald.

Guillard, F., Y. Forterre, and O. Pouliquen (2013), Depth-independent drag force induced by stirring in granular media, *Phys. Rev. Lett.*, *110*, 138,303, doi:10.1103/PhysRevLett.110.138303.

Guillard, F., Y. Forterre, and O. Pouliquen (2014), Lift forces in granular media, *Phys. Fluids*, *26*, 43,301, doi:10.1063/1.4869859.

Haefeli, R. (1939), Schneemechanik mit Hinweisen auf die Erdbaumechanik, PhD Thesis, ETHZ, Zürich, Switzerland.

Haefeli, R. (1942), Spannungs- und Plastizität Erscheinungen der Schneedecke unter besonderer Berücksichtigung der Schneedruck Berechnung und verwandter Probleme der Erdbauforschung, *Schweizer Archiv für Angewandte Wissenschaft und Technik*, *9-12*, 263–274, 308–315, 349–358, 380–396.

Haefeli, R. (1944), Zur Erd- und Kriechdruck-theorie, *Schweizerische Bauzeitung*, *123-124*, 256–260.

Haefeli, R. (1948), Schnee, Lawinen, Firn und Gletscher, in *Ingenieur-Geologie*, edited by L. Bendel, pp. 663–735, Springer, Wien.

Haefeli, R. (1951), *Neuere Entwicklungstendenzen und Probleme des Lawinenverbaus im Anbruchgebiet*, Buchdruckerei Büchler and Co., Bern, Switzerland.

Haefeli, R. (1967), Some mechanical aspects on the formation of avalanches, in *Proceedings of the International Conference on Low Temperature Science*, vol. 1, edited by H. Ôura, pp. 1199–1213, Hokkaido Univ., Hokkaido, Japan.

Hamm, E., F. Tapia, and F. Melo (2011), Dynamics of shear bands in a dense granular material forced by a slowly moving rigid body, *Phys. Rev. E*, *84*, 41,304, doi:10.1103/PhysRevE.84.041304.

Harada, Y., H. Matsushita, and M. Matuzawa (2014), Changes in design standards and regional characteristics of avalanche supporting structures in Japan, in *International Snow Science Workshop*, pp. 1014–1020, Banff, Canada. [Available at http://www.issw.net/.]

Hauksson, S., M. Pagliardi, M. Barbolini, and T. Jóhannesson (2007), Laboratory measurements of impact forces of supercritical granular flow against mast-like obstacles, *Cold Reg. Sci. Technol.*, *49*, 54–63.

Heil, P., E. C. Rericha, D. I. Goldman, and H. L. Swinney (2004), Mach cone in a shallow granular fluid, *Phys. Rev. E*, *70*, 60,301, doi:10.1103/PhysRevE.70.060301.

Heimgartner, M. (1977), On the flow of avalanching snow, *J. Glaciol.*, *19*, 357–363.

Hill, G., S. Yeung, and S. A. Koehler (2005), Scaling vertical drag forces in granular media, *Europhys. Lett.*, *72*, 137, doi:10.1209/epl/i2005-10203-3.

Höller, P. (2012), Snow gliding and glide avalanches: A review, *Nat. Hazard*, *71*(3), 1259–1288.

Höller, P., R. Fromm, and G. Leitinger (2009), Snow forces on forest plants due to creep and glide, *Forest Ecol. Manage.*, *257*, 546–552.

Holyoake, A. J., and J. N. McElwaine (2012), High-speed granular chute flows, *J. Fluid Mech.*, *710*, 35–71.

Holzinger, G., and J. Hübl (2004), Belastung eines Murbrechers abgeleitet aus Laborversuchen, in *Congress Interpraevent*, vol. 2-VII, pp. 131–139, Interpraevent Symposion, Riva del Garda, Trient.

Hu, K., F. Wei, and Y. Li (2011), Real-time measurement and preliminary analysis of debris-flow impact force at Jiangjia Ravine, China, *Earth Surf. Process. Landforms*, *36*, 1268–1278.

Huppert, H. E. (2006), Gravity currents: A personal perspective, *J. Fluid Mech.*, *554*, 299–322.

in der Gand, H. R., and M. Zupančič (1965), Snow gliding and avalanches, in *Scientific Aspects of Snow and Ice Avalanche*, vol. 69, pp. 230–242, International Association of Hydrological Sciences, Davos, Switzerland.

Isaenko, E. P. (1974), Snow avalanche impact pressure on an obstacle, in *Mécanique de la Neige*, pp. 433–440, Publication No. 114, 1975, International Association of Hydrological Sciences, Grindelwald.

Iverson, R. M. (1997), The physics of debris flows, *Rev. Geophys.*, *35*, 245–296.

Iverson, R. M. (2003), The debris-flow rheology myth, in *Debris Flow Mechanics and Mitigation Conference*, edited by C. L. Chen and D. Rickenmann, pp. 303–314, Mills Press, Davos.

Iverson, R. M. (2005), Regulation of landslide motion by dilatancy and pore pressure feedback, *J. Geophys. Res.*, *110*, F02015, doi:10.1029/2004JF000268.

Iverson, R. M., and J. Vallance (2001), New views of granular mass flows, *Geology*, *29*, 115–118.

Johnson, A. M. (1970), *Physical Process in Geology*, Freeman, Cooper, San Francisco, Calif.

Jones, A. (2004), Review of glide processes and glide avalanche release, *Avalanche News*, *69*, 53–60.

Jordan, R. E., J. P. Hardy, F. E. Perron, and D. J. Fisk (1999), Air permeability and capillary rise as measures of the pore structure of snow: An experimental and theoretical study, *Hydrol. Process.*, *13*, 1733–1753.

Jossic, L., and A. Magnin (2009), Drag of an isolated cylinder and interactions between two cylinders in yield stress fluids, *J. Non-Newtonian Fluid Mech.*, *164*, 9–16.

Katakawa, K., C. Shimomura, H. Ishikawa, S. Hatae, and H. Matsuda (1992), Characteristics of snow pressure acting on avalanche-preventive fences, in *Second International Conference on Snow Engineering*, edited by W. Tobiasson and E. Wright, pp. 323–331, USA Cold Regions Research and Engineering Laboratory, Spec. Rep. 92-27, Santa Barbara, Calif.

Katsuragi, H. (2012), Nonlinear wall pressure of a plunged granular column, *Phys. Rev. E*, *85*(2), 21,301, doi:10.1103/PhysRevE.85.021301.

Keiler, M., J. Knight, and S. Harrison (2010), Climate change and geomorphological hazards in the eastern European Alps, *Proc. R. Soc. London, Ser. A*, *368*, 2461–2479.

Kern, M. A., P. Bartelt, B. Sovilla, and O. Buser (2009), Measured shear rates in large dry and wet snow avalanches, *J. Glaciol.*, *55*, 327–338.

Kleemayr, K. (2004), Modelling and simulation in snow science, *Math. Comput. Simul.*, *66*, 129–153.

Lackinger, B. (1986), Stability and fracture of the snow pack for glide avalanches, in *Avalanche Formation, Movement and Effects*, edited by H. Gubler and B. Salm, pp. 229–241, IAHS, Wallingford, Oxfordshire, U. K. IAHS Publication No. 162, 1987, Davos.

Lackinger, B. (1988), Zum Problem der Gleitschneelawine, in *Interpraevent*, vol. 3, pp. 205–226, Graz, Austria.

Lagotala, H. (1927), *Étude de l'avalanche des Pélerins (Chamonix)*, Société Générale d'Imprimerie, Genève, Switzerland.

Larsen, J. O., J. Laugesen, and K. Kristensen (1989), Snow-creep pressure on masts, *Ann. Glaciol.*, *13*, 154–158.

Laternser, M., and C. Pfister (1997), Avalanches in Switzerland 1500–1990, in *Rapid Mass Movements Since the Holocene*, vol. 30, edited by J. Matthews, pp. 241–266, Special Issue of European Palaeoclimate and Man, 16, Stuttgart, Germany.

Lavigne, A., L. Bel, E. Parent, and N. Eckert (2012), A model for spatio-temporal clustering using multinomial probit regression: Application to avalanche counts, *Environmetrics*, *23*, 522–524.

Legros, F. (2002), The mobility of long-runout landslides, *Eng. Geol.*, *63*, 301–331.

Leitinger, G., P. Höller, E. Tasser, J. Walde, and U. Tappeiner (2008), Development and validation of a spatial snow-glide model, *Ecol. Model.*, *211*, 363–374.

Louge, M. Y., C. S. Carroll, and B. Turnbull (2011), Role of pore pressure gradients in sustaining frontal particle entrainment in eruption currents: The case of powder snow avalanches, *J. Geophys. Res.*, *116*, F04030, doi:10.1029/2011JF002065.

Margreth, S. (2007a), *Defense Structures in Avalanche Starting Zones. Technical Guideline as an Aid to Enforcement, Federal Office for the Environment*, Bern and Eidgenössisches Institut für Schnee- und Lawinenforschung, Davos, Switzerland.

Margreth, S. (2007b), Snow pressure on cableway masts: Analysis of damages and design approach, *Cold Reg. Sci. Technol.*, *47*, 4–15.

Margreth, S. (2013), When should a hazard map show the risk of small avalanches or snow gliding?, in *International Snow Science Workshop*, pp. 679–683, Grenoble, France. [Available at http://www.issw.net/.]

Margreth, S., L. Stoffel, and M. Schaer (2013), *Berücksichtigung der Lawinen- und Schneedruckgefährdung bei touristischen Transportanlagen, Bundesamt für Verkehr (BAV)*, Bern and Eidgenössisches Institut für Schnee- und Lawinenforschung, Davos, Switzerland.

Marsh, P. (1991), Water flux in melting snow covers, in *Advances in Porous Media*, vol. 1, edited by M. Y. Corapcioglu, pp. 61–124, Elsevier, Amsterdam.

Marsh, P. (2005), Water flow through snow and firn, in *Encyclopedia of Hydrological Sciences*, edited by M. G. Anderson, Part 14. Snow and Glacier Hydrology. Article 161, Wiley, New York.

Matsumoto, H., S. Yamada, and K. Hirakawa (2010), Relationship between ground ice and solifluction: Field measurements in the Daisetsu Mountains, Northern Japan, *Permafrost Periglacial Process.*, *21*, 78–89.

Matsuoka, N. (1998), Modelling frost creep rates in an alpine environment, *Permafrost Periglacial Process.*, *9*, 397–409.

Matsuoka, N. (2005), Temporal and spatial variations in periglacial soil movements on alpine crest slopes, *Earth Surf. Process. Landforms*, *30*, 41–58.

McClung, D. M. (1975), Creep and the snow-earth interface condition in the seasonal alpine snowpack, in *Symposium Mecanique de la neige. Actes du colloque de Grindelwald*, vol. 114, pp. 236–248, International Association of Hydrological Sciences, Wallingford, U. K.

McClung, D. M. (1980), *Creep and Glide Processes in Mountain Snowpacks*, National Hydrology Research Institute, Ottawa.

McClung, D. M. (1981), A physical theory of snow gliding, *Can. Geotech. J.*, *18*, 86–94.

McClung, D. M. (1982), A one-dimensional analytical model for snow creep pressures on rigid structures, *Can. Geotech. J.*, *19*, 401–412.

McClung, D. M. (1984), Empirical corrections to snow creep pressure equations, *Can. Geotech. J.*, *21*, 191–193.

McClung, D. M. (1986), Mechanics of snow slab failure from a geotechnical perspective, in *Avalanche Formation, Movement and Effects*, vol. 162, edited by H. Gubler and B. Salm, pp. 475–507, IAHS, Wallingford, Oxfordshire, U. K., and Davos, Switzerland.

McClung, D. M. (1993), Comparison of analytical snow pressure models, *Can. Geotech. J.*, *30*, 947–952.

McClung, D. M. (2013), The effects of El Niño and La Niña on snow and avalanche patterns in British Columbia, Canada, and central Chile, *J. Glaciol.*, *59*, 783–792.

McClung, D. M., and G. K. Clarke (1987), The effects of free water on snow gliding, *J. Geophys. Res.*, *B7*, 6301–6309.

McClung, D. M., and J. O. Larsen (1989), Snow creep pressures: Effects of structure boundary conditions and snowpack properties compared with field data, *Cold Reg. Sci. Technol.*, *17*, 33–47.

McClung, D. M., and P. A. Schaerer (1985), Characteristics of flowing snow and avalanche impact pressure, *Ann. Glaciol.*, *6*, 9–14.

McClung, D. M., and P. A. Schaerer (1993), *The Avalanche Handbook*, The Mountaineers, Seattle, Wash.

McClung, D. M., J. O. Larsen, and S. B. Hansen (1984), Comparison of snow pressure measurements and theoretical predictions, *Can. Geotech. J.*, *21*, 250–258.

McClung, D. M., S. Walker, and W. Golley (1994), Characteristics of snow gliding on rock, *Ann. Glaciol.*, *19*, 97–103.

Mellor, M. (1968), *Avalanches*, U.S. Army Material Command, Cold Regions Research and Engineering Laboratory, Hanover, N. H.

Mellor, M. (1978), Dynamics of snow avalanches, in *Developments in Geotechnical Engineering*, vol. 14, edited by B. Voight, pp. 753–792, Part A Rockslides and Avalanches, 1 – Natural Phenomena, Elsevier, Amsterdam.

Meusburger, K., G. Leitinger, L. Mabit, M. H. Mueller, A. Walter, and C. Alewell (2014), Soil erosion by snow gliding—A first quantification attempt in a subalpine area in Switzerland, *Hydrol. Earth Syst. Sci.*, *18*(9), 3763–3775.

Mitterer, C. (2012), Formation of wet-snow avalanches, PhD thesis, ETHZ, Zurich, Switzerland.

Mitterer, C., and J. Schweizer (2012), Towards a better understanding of glide-snow avalanche formation, in *Proceedings, 2012 International Snow Science Workshop*, pp. 610–616, Anchorage, Alaska. [Available at http://www.issw.net/.]

Moskalev, Y. D. (1967), The stability of snow cover on mountain slopes, *Inst. Low Temp. Sci.*, *A1*, 1215–1222.

Mougin, P. (1913), Correction des avalanches dans les Grisons, *Revue des Eaux et Forêts*, *52*, 513–532.

Mougin, P. (1922), *Les Avalanches en Savoie*, vol. IV, Ministère de l'Agriculture, Direction Générale des Eaux et Forêts, Service des Grandes Forces Hydrauliques, Paris.

Nedderman, R. M. (1992), *Statics and Kinematics of Granular Materials*, Cambridge Univ. Press, Cambridge, U. K.

Neto, C., R. E. Drew, E. Bonaccurso, H. J. Butt, and V. S. J. Craig (2005), Boundary slip in Newtonian liquids: A review of experimental studies, *Rep. Prog. Phys.*, *68*, 2859–2897.

Newesely, C., E. Tasser, P. Spadinger, and A. Cernusca (2000), Effects of land-use changes on snow gliding processes in alpine ecosystems, *Basic Appl. Ecol.*, *1*, 61–67.

Nicot, F. (2004), Constitutive modelling of snow as a cohesive-granular material, *Granul. Matter*, *6*, 47–60.

Nohguchi, Y. (1989), A mathematical model for instability in snow gliding motion, *Ann. Glaciol.*, *13*, 211–214.

Norem, H. (1990), Estimating snow avalanche impact pressures on towers, in *Workshop on Avalanche Dynamics, Communication No. 48*, edited by H. Gubler, pp. 42–56, Swiss Federal Institute for Snow and Avalanches, Davos, Switzerland.

Norem, H. (1992), A general discussion on avalanche dynamics, in *Université Européenne d'été sur les Risques Naturels*, edited by G. Brugnot, pp. 135–148, Cemagref, Chamonix, France.

Nye, J. F. (1969), A calculation on the sliding of ice over a wavy surface using a Newtonian viscous approximation, *Proc. R. Soc. London, Ser. A*, *311*, 445–467.

Pailha, M., M. Nicolas, and O. Pouliquen (2008), Initiation of underwater granular avalanches: Influence of the initial volume fraction, *Phys. Fluids*, *20*, 111,701, doi:10.1063/1.3013896.

Pazwash, H., and J. M. Robertson (1975), Forces on bodies in Bingham fluids, *J. Hydraul. Res.*, *13*, 35–55.

Peitzsch, E. H., J. Hendrikx, D. B. Fagre, and B. Reardon (2012), Examining spring wet slab and glide avalanche occurrence along the Going-to-the-Sun road corridor, Glacier National Park, Montana, *Cold Reg. Sci. Technol.*, *78*, 73–81.

Peitzsch, E. H., J. Hendrikx, and D. B. Fagre (2014), Assessing the importance of terrain parameters on glide avalanche release, in *International Snow Science Workshop 2014 Proceedings*, pp. 708–716, Banff, Canada. [Available at http://www.issw.net/.]

Pfeiff, C. F., and E. J. Hopfinger (1986), Drag on cylinders moving through suspensions with high solid concentration, *Physicochem. Hydrodyn.*, *7*, 101–109.

Pielmeier, C., F. Techel, C. Marty, and T. Stucki (2013), Wet snow avalanche activity in the Swiss Alps—Trend analysis for mid-winter season, in *International Snow Science Workshop*, pp. 1240–1246, Grenoble, France.

Proske, D., R. Kaitna, J. Suda, and J. Hübl (2008), Abschätzung einer Anprallkraft für murenexponierte Massivbauwerke, *Bautechnik*, *85*, 803–811.

Rabusseau, R. (2007), *Les neiges labiles: Une histoire culturelle de l'avalanche au XVIIIe siècle*, Presses d'Histoire Suisse, Genève, Switzerland.

Reardon, B. A., D. B. Fagre, M. Dundas, and C. Lundy (2006), Natural glide slab avalanches, Glacier National Park: A unique hazard and forecasting challenge, in *International Snow Science Workshop*, pp. 778–785, ISSW, Telluride, Colo.

Roch, A. (1955), Le mécanisme du déclenchement des avalanches, in *Les avalanches*, pp. 94–105, Club Alpin Suisse, Bern, Switzerland.

Roch, A. (1961), Mesure de la force des avalanches, Sonderdruck aus Winterbericht 1960/61, Nr. 25, Eidgenössisches Institut für Schnee- und Lawinenforschung, Davos, Switzerland.

Roch, A. (1980), *Neve e Valanghe*, Club Alpino Italiano, Torino.

Rudolf-Miklau, F., and S. Sauermoser (Eds.) (2011), *Handbuch Technischer Lawinenschutz*, Ernst and Sohn, Berlin.

Salm, B. (1964), Anlage zur Untersuchung dynamischer Wirkungen von bewegtem Schnee, *Z. Angew. Math. Mech.*, *15*, 357–375.

Salm, B. (1966), Contribution to avalanche dynamics, in *Scientific Aspects of Snow and Ice Avalanche*, vol. 69, pp. 199–214, IAHS Press, Wallingford, Oxfordshire, U. K., and Davos, Switzerland.

Salm, B. (1967a), An attempt to clarify triaxial creep mechanics of snow, in *Proceedings of the International Conference on Low Temperature Science*, vol. 1, edited by H. Ôura, pp. 857–874, Hokkaido Univ., Hokkaido, Japan.

Salm, B. (1967b), On nonuniform, steady flow of avalanching snow, in *Assemblée générale de Berne, Publication No. 79*, pp. 19–29, IAHS, Wallingford, Oxfordshire, U. K., and Bern, Switzerland.

Salm, B. (1977), Snow forces, *J. Glaciol.*, *19*, 67–100.

Salm, B. (1982), Mechanical properties of snow, *Rev. Geophys.*, *20*, 1–19.

Salm, B. (1993), Flow, flow transition and runout distances of flowing avalanches, *Ann. Glaciol.*, *18*, 221–226.

Salm, B., A. Burkard, and H. Gubler (1990), *Berechnung von Fliesslawinen: Eine Anleitung für Praktiker mit Beispielen*, Communication No 47, Eidgenössisches Institut für Schnee- und Lawinenforschung, Davos, Switzerland.

Sauermoser, S., M. Stoffel, and S. Margreth (2011), *Entwicklung der Lawinen und des Lawinenschutzes: Historischer Überblick*.

Scapozza, C., and P. Bartelt (2003), Triaxial tests on snow at low strain rate: Part II. Constitutive behaviour, *J. Glaciol.*, *49*, 91–101.

Schaeffer, D. G., and R. M. Iverson (2008), Steady and intermittent slipping in a model of landslide motion regulated by pore-pressure feedback, *SIAM J. Appl. Math.*, *69*, 769–786.

Schaerer, P. A., and A. A. Salway (1980), Seismic and impact-pressure monitoring of flowing avalanches, *J. Glaciol.*, *26*, 179–187.

Schneebeli, M., M. Laternser, P. Föhn, and W. J. Ammann (1998), *Wechselwirkungen zwischen Klima, Lawinen, und technischen Massnahmen*, Schlussbericht NFP 31, VDF, Zürich, Switzerland.

Schweizer, J., J. B. Jamieson, and M. Schneebeli (2003), Snow avalanche formation, *Rev. Geophys.*, *41*, 1016, doi:10.1029/2002RG000123.

Schweizer, J., K. Kronholm, J. B. Jamieson, and K. W. Birkeland (2008), Review of spatial variability of snowpack properties and its importance for avalanche formation, *Cold Reg. Sci. Technol.*, *51*, 253–272.

Seguin, A., Y. Bertho, F. Martinez, J. Crassous, and P. Gondret (2013), Experimental velocity fields and forces for a cylinder penetrating into a granular medium, *Phys. Rev. E*, *87*, 12,201, doi:10.1103/PhysRevE.87.012201.

Shapiro, L. H., J. B. Johnson, M. Sturm, and G. L. Blaisdell (1997), *Snow Mechanics: Review of the State of Knowledge and Applications*, Cold Regions Research and Engineering Laboratory, Hanover, N. H.

Shinojima, K. (1967), Study on the visco-elastic deformation of deposited snow, in *Proceedings of the International Conference on Low Temperature Science*, vol. 1, edited by H. Ôura, pp. 875–907, Hokkaido Univ., Hokkaido, Japan.

Sochi, T. (2011), Slip at fluid-solid interface, *Polymer Rev.*, *51*, 309–340.

Sommerhalder, E. (1966), Lawinenkräfte und Objektschutz, in *Schnee und Lawinen in den Schweizer Alpen. Hydrologisches Jahr 1964/1965, Winterbericht Nr. 29*, pp. 134–141, Eidgenössisches Institut für Schnee- und Lawinenforschung, Davos, Switzerland.

Sovilla, B., M. Schaer, M. A. Kern, and P. Bartelt (2008), Impact pressures and flow regimes in dense snow avalanches observed at the Vallée de la Sionne test site, *J. Geophys. Res.*, *113*, F01010, doi:10.1029/2006JF000688.

Sovilla, B., M. A. Kern, and M. Schaer (2010), Slow drag in wet-snow avalanche flow, *J. Glaciol.*, *56*, 587–592.

Sovilla, B., S. Margreth, D. Baroudi, E. Thibert, J. T. Fischer, and C. Ancey (2014), Taking into account wet avalanche load for the design of tower-like structures, in *International Snow Science Workshop*, pp. 727–732, Banff, Canada. [Available at http://www.issw.net/.]

Steinkogler, W., B. Sovilla, and M. Lehning (2014), Influence of snow cover properties on avalanche dynamics, *Cold Reg. Sci. Technol.*, *97*, 121–131.

Stimberis, J., and C. M. Rubin (2011), Glide avalanche response to an extreme rain-on-snow event, Snoqualmie Pass, Washington, *J. Glaciol.*, *57*, 468–474.

Stoffel, M., and C. Huggel (2012), Effects of climate change on mass movements in mountain environments, *Prog. Phys. Geog.*, *36*, 421–439.

Stone, M. B., D. P. Bernstein, R. Barry, M. D. Pelc, Y. K. Tsui, and P. Schiffer (2004), Stress propagation: Getting to the bottom of a granular medium, *Nature*, *427*, 503–504.

Sulzlée, C. (1950), Historique des méthodes de construction des ouvrages de protection contre les avalanches, *Revue Forestière Française*, *11*, 634–644.

Szymkiewicz, A. (2013), *Modelling Water Flow in Unsaturated Porous Media*, Springer, Germany.

Tabuteau, H., P. Coussot, and J. R. de Bruyn (2007), Drag force on a sphere in steady motion through a yield-stress fluid, *J. Rheol.*, *51*, 125–137.

Takehara, Y., S. Fujimoto, and K. Okumura (2010), High-velocity drag friction in dense granular media, *EPL*, *92*, 44,003, doi:10.1209/0295-5075/92/44003.

Techel, F., and C. Pielmeier (2011), Point observations of liquid water content in wet snow — Investigating methodical, spatial and temporal aspects, *Cryosphere*, *5*, 405–418.

Techel, F., C. Peilmeier, G. Darms, M. Teich, and S. Margreth (Eds.) (2013), *Schnee und Lawinen in den Schweizer Alpen: Hydrologisches Jahr 2011/12*, Bericht Nr. 5, WSL, Birmensdorf.

Teufelsbauer, H. (2011), A two-dimensional snow creep model for alpine terrain, *Nat. Hazard*, *56*, 481–497.

Teufelsbauer, H., Y. Wang, M. C. Chiou, and W. Wu (2009), Flow-obstacle interaction in rapid granular avalanches: DEM simulation and comparison with experiment, *Granul. Matter*, *11*, 209–220.

Thibert, E., P. Berthet-Rambaud, and D. Baroudi (2008), Avalanche impact pressure on an instrumented structure, *Cold Reg. Sci. Technol.*, *54*, 206–215.

Thibert, E., T. Faug, H. Bellot, and D. Baroudi (2013), Avalanche impact pressure on a plate-like obstacle, in *International Snow Science Workshop*, pp. 663–670, Grenoble, France. [Available at http://www.issw.net/.]

Thual, O., and L. Lacaze (2010), Fluid boundary of a viscoplastic Bingham flow for finite solid deformations, *J. Non-Newtonian Fluid Mech.*, *165*, 84–87.

Truesdell, C., and K. R. Rajagopal (1999), *An Introduction to the Mechanics of Fluids*, Birkhaüser, Boston, Mass.

Valt, M., and C. Paola (2013), Climate change in Italian Alps: Analysis of snow precipitation, snow durations and avalanche activity, in *International Snow Science Workshop*, pp. 1247–1250, Grenoble, France. [Available at http://www.issw.net/.]

Veysey, J., and N. Goldenfeld (2007), Simple viscous flows: From boundary layers to the renormalization group, *Rev. Mod. Phys.*, *79*, 883, doi:10.1103/RevModPhys.79.883.

Viglietti, D., M. Maggioni, E. Bruno, E. Zanini, and M. Freppaz (2013), Snow gliding and loading under two different forest stands: A case study in the north-western Italian Alps, *J. Forest. Res.*, *24*, 633–642.

Voellmy, A. (1955a), Über die Zerstörungskraft von Lawinen, *Schweizerische Bauzeitung*, *73*, 159–165.

Voellmy, A. (1955b), Über die Zerstörungskraft von Lawinen: III. Stau- und Druckwirkungen, *Schweizerische Bauzeitung*, *73*, 246–249.

Walter, B., S. Horender, C. Gromke, and M. Lehning (2013), Measurements of the pore-scale water flow through snow using Fluorescent Particle Tracking Velocimetry, *Water Resour. Res.*, *49*, 7448–7456, doi:10.1002/2013WR013960.

Weertman, J. (1979), The unsolved general glacier sliding problem, *J. Glaciol.*, *23*, 97–115.

Wieghardt, K. (1975), Experiments in granular flow, *Annu. Rev. Fluid Mech.*, *7*, 89–114.

Zakeri, A. (2009), Review of state-of-the-art: Drag forces on submarine pipelines and piles caused by landslide or debris flow impact, *J. Offshore Mech. Artic. Eng.*, *131*, 14,001, doi:10.1115/1111.2957922.

Zanuttigh, B., and A. Lamberti (2006), Experimental analysis of the impact of dry avalanches on structures and implication for debris flows, *J. Hydraul. Res.*, *44*, 522–534.

Zanuttigh, B., and A. Lamberti (2007), Instability and surge development in debris flows, *Rev. Geophys.*, *45*, RG3006, doi:10.1029/2005RG000175.

Zarraga, I. E., D. A. Hill, and D. T. Leighton (2000), The characterization of the total stress of concentrated suspensions of noncolloidal spheres in Newtonian fluids, *J. Rheol.*, *44*, 185–221.

Zhang, S. (1993), A comprehensive approach to the observation and prevention of debris flows in China, *Nat. Hazard*, *7*, 1–23.